Mechanistic insights into global suppressors of protein folding defects

Gopinath Chattopadhyay[1#], Jayantika Bhowmick[1#], Kavyashree Manjunath[2], Shahbaz Ahmed[1], Parveen Goyal[2], Raghavan Varadarajan[1*]

[#] These authors have contributed equally

[1]Molecular Biophysics Unit, Indian Institute of Science, Bangalore-560012, India
[2]Institute for Stem Cell Science and Regenerative Medicine, Bangalore 560065, India
[*]Corresponding Author
Raghavan Varadarajan, Molecular Biophysics Unit, Indian Institute of Science, Bangalore, 560012 (INDIA), *Email*: varadar@iisc.ac.in, PHONE: +91-80-22932612, FAX: +91-80-23600535

Running Title: Mechanism of global suppression.

Number of manuscript pages: 81

Number of supplementary figures: 6

Number of figures: 8

Number of supplementary tables: 10

Number of tables: 1

Abstract:

Most amino acid substitutions in a protein either lead to partial loss of function or are near neutral. Several studies have shown the existence of second-site mutations that can rescue defects caused by diverse loss of function mutations. Such global suppressor mutations are key drivers of protein evolution. However, the mechanisms responsible for such suppression remain poorly understood. To address this, we characterized multiple suppressor mutations both in isolation and in combination with inactive mutants. We examined five global suppressors of the bacterial toxin CcdB, the known M182T global suppressor of TEM-1 β-lactamase, the N239Y global suppressor of p53-DBD and three suppressors of the SARS-CoV-2 spike Receptor Binding Domain. The suppressors both alone, and in conjunction with inactive mutants, stabilise the protein both thermodynamically and kinetically in-vitro, predominantly through acceleration of the refolding rate parameters. When coupled to inactive mutants they promote increased in-vivo solubilities as well as regain-of-function phenotypes. Our study also demonstrates that the global suppressor approach can be used to consistently stabilise wild-type proteins, including for downstream translational applications.

Keywords: global suppressor, protein stability, refolding, unfolding kinetics, thermal tolerance, aggregation, vaccine.

Introduction

Certain specific interactions influencing a protein's structure and function are preserved throughout evolution, either by conservation of the interacting pair, or by mutation of the pair in a correlated fashion (1). Correlated mutational data extracted from multiple sequence alignments, can guide structure prediction of a protein (2) or help in the determination of interfacial residues responsible for binding to various partners (3). Experimental studies have often led to the identification of second suppressor mutations which can alleviate the defects in folding, function and stability of the protein caused by an initial deleterious mutation. Such compensatory mutations, often occur within the same gene, highlighting the role of intragenic suppression in evolution (4).

Suppressors can be either spatially proximal or distal to the inactivating mutation. Distal suppressors are typically able to suppress multiple inactivating mutations, not necessarily in proximity to each other. Hence distal suppressors are often referred to as global suppressors. Prior studies on distal suppressors have shown that such suppressors function either by (a) increasing global thermodynamic stability (5), (b) enhancing the activity of the native protein without any effect on stability (6), or (c) improving the folding of the native protein without substantial enhancement of the thermodynamic stability (7). In laboratory-based evolution experiments, it has been shown that the evolution of new function is accompanied by second-site compensatory mutations, which compensate for the probable destabilizing function altering mutations (8). Previous studies have primarily focused on thermodynamic rather than kinetic effects of mutations on protein stability and function, though the latter may be more relevant *in vivo* (9).

Here, we endeavour to provide insights into the mechanisms responsible for global suppression. The primary experimental system utilised is a 101-residue homo-dimeric protein CcdB (Controller of Cell Death protein B), which is a part of the toxin-antitoxin (CcdB-CcdA) module, involved in the maintenance of F-plasmid in *E. coli* (10). We probe effects of multiple global suppressors of CcdB, on the folding kinetics, stability, *in vivo* solubility and *in vivo* activity of the protein. The suppressors are

able to rescue folding defects of the inactive mutants, through thermodynamic and kinetic stabilization, with the largest effects on the refolding rate. We also determined the structure of three of the CcdB suppressors mutants, S12G, V46L and S60E using X-ray crystallography to understand the structural basis of stabilization. We probed the effect of the suppressor mutants on aggregation, binding and thermal tolerance. Molecular Dynamics (MD) simulations were employed to investigate changes in flexibility of the CcdB mutants at 293 K and 313 K relative to the WT. We also examined the effects on stability and folding of two known global suppressors: M182T of TEM-1 β-lactamase, an extended spectrum β-lactamase (ESBL) enzyme conferring antibiotic resistance against third generation cephalosporins and N239Y in the DNA binding domain (DBD) of p53, a critical tumour suppressor protein, which is known to suppress the effect of oncogenic inactive mutants. We further examined the effects of additional suppressor mutations that were recently isolated for CcdB and RBD (Receptor Binding Domain of spike glycoprotein of SARS-CoV2), on protein stability and folding. The analysis of data for these diverse systems revealed insights into the mechanism of action of global suppressors.

Results

Identification of second-site suppressor mutations of CcdB

In order to achieve tuneable expression levels using arabinose (inducer) and glucose (repressor), the *ccdB* gene was cloned under control of the pBADAraC promoter in the pBAD24 vector (11). A previously described single site saturation mutagenesis (SSM) library of ~1600 mutants includes several single mutants that lead to partial or complete loss of function (9,12,13). Five such mutants, termed parent inactive mutants (PIMs), (namely V5F, V18W, V20F, L36A and L83S) were chosen for further study. Next, exhaustive second-site saturation mutagenesis libraries were constructed by incorporating each of the PIMs into the original SSM library. PIMs bound GyraseA poorly. In order to identify the suppressors of the PIMs, suppressor libraries were then displayed on the yeast surface and screened for improved binding to GyraseA by FACS (2). In the study, two residues R10 and

E11 on an exposed loop region were also identified as distal suppressors (Figure 1A). The global suppressor R10G was able to suppress defects at all the five positions and was also shown to increase the T_m by 8 °C, relative to WT CcdB (2) but E11R was not characterized. Recently, another possible global suppressor S12G was identified (14). S12, located on an exposed loop, along with R10 and E11, is involved in hydrogen bonding with the cognate antitoxin CcdA (Figure 1A). The aim of the present study was to experimentally validate whether these mutations (S12G, E11R) also stabilise WT CcdB and to understand possible mechanisms responsible for the suppressor phenotypes. The study involves characterization of these putative global suppressors both individually and in the context of several known inactive mutants.

CcdB suppressors rescue the folding defects and restore activity of the inactive mutants *in vivo*

***In vivo* activity and solubility of the inactive mutants in the background of suppressors:** The phenotype of the CcdB mutants were studied after transforming the plasmids individually into the *Top10*pJAT strain which is sensitive to CcdB toxin action. The cells were allowed to grow at different concentrations of glucose and arabinose (9,13) to allow increasing levels of expression of CcdB from the P_{BAD} promoter. Mutant phenotypes were studied as a function of varying repressor (glucose) and inducer (arabinose) concentration. For WT and the fully active mutants E11R and S12G, the cells fail to grow even at the highest glucose (repressor) concentration (0.2% glucose). On the other hand, the inactive mutants grow even at the highest concentration of arabinose (0.2% arabinose). However, in the background of the E11R or S12G mutations, with the exception of V18W-S12G, the WT phenotype of the remaining (PIM, suppressor) pairs is restored at lower ara concentrations (≥ 0.02%), leading to cell death (Figure 1B).

For proper function, proteins need to fold into their native structure avoiding misfolding or formation of aggregates. To examine the relative solubility levels, *E. coli* strain *Top10GyrA* was individually transformed with each mutant. The solubilities of the PIMs were significantly lower than that of WT CcdB and suppressors E11R and S12G (Table S1). However, the solubilities of the inactive mutants

in the background of the suppressors was significantly enhanced (Figure S1A). These results reveal that lowered activity and decrease in solubility of the inactive proteins are both improved in the background of the suppressors.

Enhancement of thermal and chemical stability of multiple inactive mutants by global suppressors

The WT and CcdB mutants were purified by affinity purification against immobilised ligand CcdA. Yield for all mutants varied from 0.3-12 mg/L depending upon the amount of protein in the soluble fraction. V5F and V5F-S12G could not be purified because of their low expression, solubility and inability to bind to the CcdA column. V18W-E11R and V20F-E11R could not be used for further biophysical studies owing to their high tendency to aggregate.

The purified proteins (4 μM) were subjected to thermal denaturation using nanoDSF and the apparent T_m was calculated (Figure 1D). S12G had a 2 °C higher T_m, indicating that the mutation is stabilising (Table S1). Further the inactive mutant-suppressor pairs showed increased apparent thermal stabilities (~5-12 °C) relative to the inactive mutants. The ability of the purified proteins to bind to CcdA peptide (8 μM) was also examined by monitoring thermal denaturation using binding of Sypro orange dye (15), both in the absence and presence of CcdA peptide (45-72). Relative to the free proteins, apparent T_m's of the CcdA-bound complexes showed increments (Figure S1B) due to stability-enhancements of the proteins in the presence of peptide (2).

Equilibrium unfolding experiments for the CcdB mutants were carried out by nanoDSF. The data were fitted to $N_2 \leftrightarrow 2D$ unfolding models for the homo-dimeric CcdB. The fraction unfolded of different CcdB mutants (200 mM HEPES, pH 8.4) in presence of GdnCl is plotted as a function of denaturant concentration (Figure 1C). The midpoint of chemical denaturation (C_m), ΔG^o and m-values were measured for all the CcdB mutants (Table S5). The suppressor S12G alone is 0.8 kcal/mol more stable than the WT, and the double mutants are apparently 2.5-5.0 kcal/mol more stable than the inactive mutants (Figure 1D). The significant difference in the apparent effect of the suppressor in the context

of PIM relative to WT, is likely due to the high tendency of inactive mutants to aggregate over time thereby reducing the amount of functionally folded form. The E11R is 3.1 kcal/mol less stable than the WT protein. This is surprising because their thermal stabilities are similar and E11R is able to enhance the stability of multiple PIMs by 4-5 kcal/mol. Being a charge reversal mutation, the pI of the protein was changed significantly (6.1 to 8.1) which accounts for the visible aggregation of the E11R mutant at 200 mM HEPES, pH 8.4. Hence, the chemical denaturation and folding kinetics of E11R and WT were repeated in PBS (pH 7.4) where E11R behaves similar to the WT protein (Figure S1 C-H, Table S4).

Suppressor substitutions accelerate the refolding rate and reduce the unfolding rate of the WT and multiple inactive mutants

Refolding and unfolding kinetics for CcdB mutants were also monitored by time-course fluorescence spectroscopy at 25 °C using nanoDSF. Refolding was performed at pH 8.4, at final GdnCl concentrations ranging from 0.5 M-1.5 M. During refolding, the two monomers rapidly associate in a diffusion limited process (16). Refolding for the WT occurs with a fast and a slow phase as observed earlier (16). The suppressors E11R and S12G alone refold at a faster rate compared to the WT. Relative to the WT, the inactive mutants refold slowly, whereas their refolding rates were enhanced (both fast and slow phase) in the background of the suppressor (Figure 2A, Table S2).The fast phase of refolding for L83S-E11R could not be captured owing to its fast refolding kinetics. The unfolding trace of WT CcdB when fitted to the three-parameter unfolding equation, gives a fitted unfolding rate of 0.05 s^{-1}. S12G shows a much slower rate of unfolding. For all the PIMs ,we observed very fast unfolding even at low GdnCl concentrations whereas the mutant-suppressor pairs had slower unfolding rates relative to the individual PIMs, though typically faster than the rates for WT and the suppressors E11R and S12G (Figure 2B,Table S2). Refolding and unfolding reactions were carried out at three different GdnCl concentrations and the observed rate constants and m values were plotted as a function of GdnCl concentration (Figure S2, Table S3).Using this, the refolding rate constants for both fast and slow

phases and unfolding rate constants were calculated at 0 M GdnCl as described previously (17) for relative comparison (Table S3). These experiments correlate with other results and indicate that the suppressors E11R and S12G have similar to marginally higher thermal stabilities than WT and that all the mutant-suppressor pairs are both kinetically and thermodynamically more stable than the corresponding PIMs.

Rescue of activity and stability of refolded CcdB proteins by the global suppressors

The affinity of fluorescently labeled Gyrase to CcdB mutant proteins (native, native in GdnCl and refolded proteins) was analysed using MST. The assays were carried out with a fixed concentration of the labeled Gyrase (70 nM), which was titrated with different concentrations of the unlabeled CcdB mutants. The obtained data indicates that WT CcdB, S12G and E11R bind GyraseA14 with K_D's of about 2.2, 2.3 and 1.2 nM respectively which is consistent with the SPR binding studies (Figure 2C, S3A, Table S1). Labeled Gyrase also bound with similar affinity to the native and refolded proteins in 1.5 M GdnCl (Figure 2C, S3B-C Table S1), indicating that refolding was reversible. The C_m of Gyrase was determined to be 4.48 M, confirming that it was folded at 1.5 M GdnCl used in the above refolding assay (Figure S3D).

The refolded CcdB proteins and the native proteins in the presence of 1.5 M GdnCl were also subjected to thermal denaturation, and the apparent T_m was calculated (Figure 2D, Table S5). Except for the PIMs V18W and V20F, all the other mutants showed clear thermal transitions confirming that they were in a folded conformation in the presence of GdnCl. The suppressors improved the T_m of the refolded proteins, relative to the PIMs.

Enhancement of Thermal tolerance of the CcdB mutants by the global suppressors

The binding of purified CcdB mutants to their target Gyrase, was also probed using SPR. WT CcdB, S12G and E11R bind to Gyrase with K_D's of about 1.4, 2.6 and 2.8 nM respectively (Figure S4, Table S1). An increased affinity for DNA Gyrase for the inactive mutant-suppressor pairs was observed in

all the cases. This explains the ability of these suppressors to rescue the activity of the inactive mutants, which are defective in binding and poisoning DNA Gyrase. The apparent low affinity of these inactive mutants may also arise due to the inability to estimate the fraction of active protein for these purified mutants. The SEC profile of the PIM L36A, shows a significant amount of aggregation as well as degradation as compared to the WT, suppressor S12G and the double mutant L36A-S12G (Figure 2F). For the other mutants, due to poor yields and high tendency to aggregate, SEC was not performed. Thermal tolerance of the mutants E11R, S12G, L36A, L36A-E11R,L36A-S12G and WT CcdB, was also assessed by determining the binding of CcdB proteins to Gyrase after prolonged heat stress followed by cooling to room temperature (Figure 2E, Table S5). The S12G mutant retained 4% activity after incubation at 80 °C for 1hr, representing a five-fold improvement over WT, whereas the double mutants L36A-E11R and L36A-S12G showed three-fold and ten-fold improvement over WT respectively. Surprisingly, L36A-E11R had residual activity at 40 °C, as compared to E11R alone.

MD simulation shows reduced flexibility of the S12G mutant at both 293K and 313K

The S12G was experimentally found to be thermally stable compared to the WT protein. To obtain further insights, WT CcdB and the mutants E11R, S12G, L36A, L36A-S12G were simulated as biological dimers for 50 ns at temperatures of 293K and 313K. The root mean square deviation (RMSD) calculations of the Cα atoms of the structures (dimer), from the starting reference structures, indicated greater deviations in WT and L36A, both at 293K and 313K compared to S12G, E11R and L36A-S12G (Figure 3A) indicating features of instability. The PIM L36A had two distinct clusters at both the temperatures as observed from the RMSD distributions whereas the WT showed two distinct clusters at 313 K, while the S12G, E11R, L36A-S12G exists as a single cluster (Figure 3B). The S12G, E11R and L36A-S12G structures cluster at a lower RMSD compared to WT and L36A at both temperatures pointing to the overall dynamic stability of S12G, E11R and L36A-S12G structures. The WT and L36A structures at 313K also showed higher RMSF (root mean square fluctuation) around the residues 9-11, 41-50, 56-61 (Figure 3C). The pronounced difference in WT and L36A as compared

to S12G, E11R, L36A-S12G (313K), points to the possibility of stabilization of distant regions specifically loop 40-60 which is less flexible in S12G, E11R and L36A-S12G (Figure 3D-E).

Thermodynamic and kinetic stabilisation mediated by the M182T global suppressor substitution in extended spectrum TEM-1 β lactamases conferring antibiotic resistance

TEM-1 β-lactamase, a 263 residue monomeric enzyme confers resistance to β-lactam antibiotics (18). There have been several studies on its stability and folding kinetics making it a suitable system to study the effect of global suppressor substitutions (19,20). M182T found frequently in clinical isolates in combination with other mutations (R164, E104, M69I, R244) is far from the active site but it restores the stability defects caused by the substitutions near the active site, resulting in increased protein expression and thereby conferring drug-resistance in clinical isolates, resulting in extended spectrum β-lactamase (ESBL) (Wang et al., 2002). It was previously shown that M182T was able to rescue the folding defect in a naturally isolated variant M69I, thus conferring resistance to inhibitors such as clavulanate (Inhibitor-resistant TEM β-lactamases, IRTs) as well as in a core engineered substitution L76N, a position which has been shown to be sensitive to substitutions (7,22) with M182T being distant from the primary mutation (Figure 4A).

In the present study, we characterised the global suppressor M182T and observed its effect on stability and folding of known inactive mutants (Figure 4). We determined the MIC and IC_{90} of the TEM-1 WT, M182T, M69I, M69I-M182T, L76N and L76N-M182T for both ampicillin and cefotaxime, a third-generation cephalosporin (Figure 4B-C, Table S6). In line with a previous study, we found that the M182T suppressor alone and the M69I-M182T double mutant have comparable values to that of the WT (23) and M69I respectively (24), however M182T rescues the activity of the inactive enzyme mutant L76N (Figure 4B-C Table S6) (22,25). Further the activity of the purified mutants was monitored *in vitro* with nitrocefin (Figure 4D). The results obtained showed similar effects of the M182T substitution on WT or M69I or L76N background as observed *in vivo* (Figure 4D and S5C-E).

The M182T suppressor substitution enhanced both the thermal and chemical stability of the WT protein as well as the inactive mutants M69I and L76N (Figure 4E-F, Table S6), in agreement with previously published results (26). When compared with WT, M69I and L76N are less stable (Figure 4G). The suppressor alone is 6 °C, 1.8 kcal/mol more stable than the WT, and M69I-M182T and L76N-M182T are 7 °C, 2 kcal/mol and 8 °C, 1.7 kcal/mol more stable than the inactive mutants M69I and L76N respectively (Figure 4G).

Refolding (in 0.5 M GdnCl) and unfolding (in 2.5 M GdnCl) kinetics for all the mutants (5 μM) were also monitored using nanoDSF, in 10 mM HEPES, 300 mM NaCl, 10% glycerol, pH 7.0, at 25 °C. The unfolding trace of WT TEM-1 when fitted to the three-parameter unfolding equation, gives a fitted unfolding rate of 0.03 s^{-1}. M182T shows a slightly slower rate of unfolding whereas the inactive mutants M69I and L76N, had two and three fold faster unfolding rates respectively as compared to the WT. The mutant-suppressor pairs however had a slower rate of unfolding as compared to the individual inactive mutants (Figure 4H and S5B, Table S6). The refolding rate constants for each of these mutants, were also calculated for both fast and slow phases. The M182T suppressor alone, refolds at a faster rate compared to the WT. The inactive mutants showed slower refolding kinetics than the WT. In the background of the suppressor, however the inactive mutants refold at a faster rate (both fast and slow phase) (Figure 4I and S5A, Table S6).

The refolded TEM-1 proteins and the native proteins in the presence of 0.5 M GdnCl were also subjected to thermal denaturation, and the apparent T_m was calculated (Figure 4J, Table S6) which was similar in both the cases. Except for the inactive mutant L76N, all the other mutants showed a proper transition indicating that they were in a folded conformation in the presence of GdnCl and the T_m of the refolded suppressors were also higher than the corresponding inactive mutants (Figure 4J). Further, lactamase activity of native and refolded proteins, both in 0.5 M GdnCl, checked by nitrocefin hydrolysis yielded results consistent with the other studies (Figure 4D and S5C-E).

These experiments indicate that the M182T suppressor alone and in the mutant-suppressor pairs (M69I-M182T and L76N-M182T) rescues the folding defects of inactive mutants and confers higher thermodynamic and kinetic stability relative to the inactive mutants. This is in contrast to a previous study (7) which indicated that the L76N-M182T double mutant was destabilized relative to the L76N inactive mutant, despite the fact that the double mutant showed higher activity *in vivo*. We show that the major contribution to stability mediated by the M182T suppressor substitution is a high refolding rate which allows reversible refolding, even in the background of the inactive mutants.

Rescue of common oncogenic mutations by an N239Y global suppressor in p53-DBD

The transcription factor, p53, acts as a tumor suppressor with multiple anti-proliferative functions upon activation in response to various upstream cellular stress signals (27) Owing to the low thermodynamic stability (28) of its core , DNA Binding Domain (DBD), nearly half of all the human cancers are associated with inactivated p53 proteins, where the mutations primarily located in this domain, destabilise or distort the DBD (Cañadillas et al., 2006). The basis of such oncogenic mutations can be structural or functional (30). Previous studies have identified second-site suppressor mutations in the DBD which could restore the WT p53 functionality (31). One such suppressor mutation, N239Y in the L3 loop of the DBD, could globally rescue multiple missense mutations located at varying regions of the protein by thermodynamic stabilisation of the inactivated core (28,30). The activity of two of the destabilising oncogenic mutations, located in the core of the DBD, V143A and V157F, have been restored by N239Y- (27,28,30,32).

In the current study, we aimed to obtain mechanistic insight into the N239Y-mediated suppression of the inactivated p53 mutations, V143A and V157F (Figure 5A). The double mutants V143A-N239Y and V157F-N239Y showed enhanced expression in the soluble fraction *in vivo* in *E. coli*, relative to their corresponding inactive mutants. WT and N239Y single suppressor mutant showed comparable soluble expression and yield (Figure 5B). The inactive mutants, V143A and V157F, owing to their low expression levels and aggregation-prone natures, could not be purified or characterised. N239Y, in

isolation and in conjunction with the inactive mutants, marginally enhanced the thermal and chemical stabilities of the WT p53 (Figure 5C-D, Table S7). Relative to the WT protein, the suppressor N239Y alone, and the mutants, V143A-N239Y, V157F-N239Y enhance the apparent thermal stabilities by ~1.3 °C, 1 °C and 3 °C respectively. The N239Y, V143A-N239Y and V157F-N239Yhave marginal increments in their thermodynamic stabilities over the WT protein in the range of ~ 0.1 -0.4 kcal/mol (Figure 5E).

Refolding (in 2 M urea) and unfolding (in 4.4 M urea) kinetics for the WT and mutants were monitored using nanoDSF at 15 °C. The unfolding traces, fitted to five-parameter unfolding equations, yielded comparable slow-phase unfolding rates for the WT and N239Y proteins (0.003s^{-1} and 0.0025 s^{-1} respectively), whereas the unfolding rates for the double mutants were slightly lower than that for the WT (0.0017 s^{-1} for V143A-N239Y and 0.0019 s^{-1} for V157F-N239Y) (Figure 5F and S5G, Table S7). The fast-phase unfolding rates for the single and double mutants were marginally lower than that for the WT (Table S7). The refolding traces, also fitted to five-parameter equations, yielded slow-phase refolding rates which were remarkably increased by ~20 and ~10 folds for N239Y and V143A-N239Y respectively, relative to the WT. V157F N239Y refolded with a similar slow-phase rate constant, when compared with the WT. With respect to the fast phase , V157F-N239Y refolds faster than the WT by ~ 3.5 folds, whereas the N239Y and V143A-N239Y refold with similar or marginal increments when compared with the WT (Figure 5G and S5F, Table S7).

The thermal denaturation of the refolded p53 proteins, along with the native proteins in 0.5 M urea as controls were also studied (Figure 5H). All the mutants showed a proper transition indicating that they were in a folded conformation in the presence of Urea. ~ 3 °C increment was observed for the apparent T_m of refolded V157F-N239Y relative to that of the refolded WT, whereas the apparent T_m's for the refolded proteins of N239Y and V143A-N239Y were similar to that for the refolded WT (Figure 5H, Table S7).

These observations indicated that the N239Y suppressor mutation likely rescues the inactivated destabilised p53 core by marginal enhancement of the thermodynamic and more importantly the kinetic stability of the proteins containing the suppressor, with the largest effect on the refolding rates.

Effect of global suppressor substitutions in WT background

In order to further, investigate the role of suppressors in the protein stability in the WT background, we performed detailed thermodynamic and kinetic studies of the suppressors alone in CcdB and mRBD proteins (Figure 6).

In a separate study from our lab, along with S12G, several other suppressor substitutions were also identified from yeast surface display (14). In the present study, we selected three such suppressor substitutions, Y8D, V46L and S60E with ΔT_m>3 °C (Figure 6A). The purified proteins were subjected to chemical denaturation (Figure 6B). The suppressors Y8D, V46L and the suppressor S60E were ~3 kcal/mol and ~4 kcal/mol respectively more stable than the WT (Figure 6C, Table S8). The suppressors were also subjected to unfolding (in 4.5 M GdnCl) and refolding (in 2 M GdnCl) kinetic studies. The unfolding rates of the suppressors were 2-2.5 times slower than the WT (Figure 6D and S6B, Table S9), whereas the fast and slow phase refolding rates of the suppressors were 2-5 times and 9-14 times faster than the WT respectively (Figure 6E and S6A, Table S9). Further, the proteins were refolded in 1, 2, 3 and 4 M GdnCl and subjected to thermal denaturation. Native protein at the same GdnCl concentrations was used as control (Figure 6F and S8). The WT could refold back till 2 M GdnCl, whereas the suppressors Y8D, V46L and suppressor S60E could refold even at 3 and 4 M GdnCl respectively (Figure S6E-H). In all cases, the refolded proteins have a broader transition than the native proteins in GdnCl, likely due to the formation of aggregates during refolding.

Next, we investigated the role of the suppressor substitutions in the context of the receptor binding domain (RBD) of SARS-CoV-2 (33). We recently also identified three suppressors of folding defective mutants in this protein. These suppressors, D389E, L390M and P527I when introduced into WT mRBD have ΔT_m≥3 °C (Figure 6G). The purified suppressors were subjected to chemical denaturation

(Figure 6H). In a separate study we have seen that WT mRBD unfolds via a three-state transition during chemical denaturation. In the present study, the suppressors D389E, L390M and P527I were ~0.2-0.4 kcal/mol more stable than the WT for the intermediate to unfolded state (I-U) transition. For the native to intermediate state (N-I) transition, the suppressors D389E, L390M and P527I were ~0.4-0.7 kcal/mol more stable than the WT (Figure 6I, Table S8). The suppressors were also subjected to unfolding (in 3 M GdnCl) and refolding (in 0.5 M GdnCl) kinetic studies. The unfolding rates of the suppressors were marginally slower than the WT for both fast and slow phases (Figure 6J and S6D, Table S9), whereas the refolding rates of the suppressors were 2.5-7 times faster than the WT (Figure 6K and S6C, Table S9). Further, the proteins were refolded in 0.5, 1, and 2 M GdnCl and subjected to thermal denaturation with native proteins in the same GdnCl concentrations as control (Figure 6L). The WT could refold back till 1 M GdnCl, whereas the suppressors D389E, L390M and P527I refolded back till 2 M GdnCl (Figure S6I-K). The binding of the native proteins, native proteins in 0.5 M GdnCl and refolded proteins in 0.5 M GdnCl with ACE2-hFc neutralizing antibody were also measured using ProteOn (Figure 6M). All the refolded proteins showed binding to the ACE2-hFc, indicating that the proteins were properly refolded back to their functional conformation (Figure S6L-O).

Structural insights into the stability of CcdB suppressor mutants

The structure of the S12G, V46L and S60E mutants of CcdB was solved to resolutions of 1.63 Å, 1.35 Å and 1.93 Å respectively. (Figure 7). For further validation, the crystals were dissolved in water and the mass was confirmed by ESI-MS.

The structures of S12G, V46L and S60E (Figure 7A, 7D, 7G) consist of a single chain in the asymmetric unit, with two chloride ions. One of the ions, which is also present in the WT structure 3VUB, interacts electrostatically with H85[Nε2], R86[NH1], H55[N] and a hydrogen bonding interaction with a symmetry equivalent T7[Oγ1]. The second Cl^- ion in S12G interacts with S38[N], R15[NH2] and a water O[220]. Although there is a water molecule at this position in the wild type structure (3VUB), addition of a water in S12G resulted in an unusually low B-factor whereas a Cl^- ion

fits well without any negative density and a B-factor of 20 $Å^2$. The density for the last residue I101 was not visible in the map for S12G. The electron density map in the region of residues 40-45 for S12G, 43-45 for V46L and 41-42 for S60E was very poor, as a result the side chains could not be fitted. One of the residues in S12G, R40 lies outside but close to the allowed region of the Ramachandran Plot. The mutant structures are very similar to the wild type structure (3VUB) with an RMSD of 0.26, 0.39 and 0.39 Å for S12G (Figure 7B), V46L (Figure 7E) and S60E (Figure 7H) respectively.

For S12G, the variation is mainly in the loop region between Y8-Y14 and A39-V46, indicated in Figure 7B by a star. There are two water molecules (254 and 228) in S12G in place of the two conformers of S12[OH] of 3VUB (Figure 7C). A cluster of water molecules at a hydrogen bonding distance from G12 stabilizes the loop and anchors it via interactions with the backbone atoms of neighbouring residues (Figure 7C) reducing the average B-factor in this region (Figure 7J). These two water molecules substitute for the hydroxyl group of both the conformers of serine in the WT structure. Sine the S12G has an additional Cl^- ion, an additional comparison was done with the structure 4VUB (WT CcdB) which has the second Cl^- ion in the same position as found in S12G. It was found that although the absolute B-factor of S12G and 4VUB were similar in the 8-12 region and lower than that of 3VUB, it was lowest for S12G in the region 39-46 amongst the three structures.

For V46L, the loop region A39-V46, exhibits a major deviation from WT CcdB, as indicated in Figure 7E by a star. L46 is involved in a hydrogen-bond interaction with R62 and hydrophobic interactions with M64 (Figure 7F). The hydrogen-bond interactions are formed between the main chain oxygen atom of L46 and side chain nitrogen atoms of R62 (NH1, NH2). The average B-factors of the V46L structure are lower than the WT with the most reductions in the loops 8-14 and 39-46 (Figure 7J).

For S60E also the major deviation, is in the starred loop region A39-V46 (Figure 7h). E60 is involved in a series of salt-bridge interactions with R48, H55 and R62 (Figure 7I). The salt bridge interactions are formed between the side chain oxygen atoms of E60 (OE1 and OE2) and side chain nitrogen atoms

of R48 (NE, NH1), H55 (ND1, NE1) and R62 (NE). There is a change in the orientation of the mobile R48 side chain resulting in salt bridge interactions with E60 (Figure 7I). The S60E mutation has resulted in reduced B-factor differences between the side chain and main chain in many regions, including R48, resulting in overall stabilisation of the structure. The average B-factors of the S60E structure are also lower than the WT with the most reductions in the loops 8-14 and 39-46 (Figure 7J).

Discussion

In this work we examine the mechanisms by which a second (suppressor) mutation alleviates the protein defects caused by the initial loss of function causing point mutant (Figure 8). The studies have shown physically interacting residues to coevolve (34). For a pair of residues in contact, the compensation of stability caused by a defect at one position occurs by shape or charge complementarity at a nearby site in the protein core (2). The location of suppressor mutations may be either spatially proximal or distal from the site of the original mutation. Unlike their proximal counterparts, distal suppressors are generally found on the surface of the protein (35), and are expected to have a WT like phenotype, when present as single mutants (2). Global suppressors are versatile mutations that can rescue the protein from damage caused by a number of non-functional point mutants, located in diverse regions of the structure. Some plausible mechanisms responsible for global suppression are: a) improving the foldability of the protein without impacting stability (7), b) increasing global thermodynamic stability (5,36,37) thereby compensating a folding defect caused by an initial destabilising albeit function altering mutation (Brown et al., 2010; Bershtein et al., 2008; Tokuriki and Tawfik, 2009), c) improving the specific activity of the protein, for example through a mutation at a functionally important residue (6).

A recent deep sequencing analysis of the SSM library in the background of different PIMs, revealed the presence of several other putative global suppressors, including S12G. In the present study we characterised the mechanisms of suppression by E11R and S12G in considerable detail, and extended

these studies to three other global suppressors, Y8D, V46L and S60E. Non active-site, buried mutations typically affect the levels of correctly folded protein (40). The presence of low levels of active, folded CcdB protein is sufficient to kill the cells and rescue the inactive phenotype caused by the PIMs. This was confirmed *in vivo* by growth assays and estimation of solubility levels. Equilibrium thermal and chemical denaturation studies reveal a large enhancement in the apparent stability of PIM-suppressor proteins with respect to the PIMs in isolation. These observations might explain a part of the suppression mechanism by the compensation of stability defects, as stated above (5,41). Surprisingly, addition of the suppressor mutation E11R does not improve the stability of WT CcdB, and the S12G mutation shows a marginal improvement in stability. There is however, a surprising non-additivity of the apparent stabilising effect of E11R in the presence and absence of the PIM. This might be attributed to the fact that the stability of the PIMs are difficult to measure accurately because of their aggregation-prone nature.

Kinetic studies were used to further elucidate the mechanism of action of such distal global suppressors. For a protein to remain functional on biologically-relevant time scales, apart from thermodynamic stability, kinetic stabilization plays a significant role (42). Several studies have shown the importance of kinetic stability in the evolutionary optimization of the protein function (43); regulation of activity of several membrane fusion proteins and transcription factors (Bullough et al, 1994; Chan et al., 1997a; Lee et al., 2000), functioning of collagen under physiological conditions (47,48) and in detailed studies of the relation between genotype and phenotype (9). Kinetic destabilisation leads to diseases associated with protein misfolding (49,50). Therefore, a mutation which enhances kinetic stability is indeed important in both physiological and pharmaceutical contexts, for example increasing shelf life of monoclonal antibodies (Ionescu *et al*, 2008). The refolding rates for the suppressor pairs are enhanced significantly compared to their PIM counterparts. A dramatic decline in the rates of unfolding is clearly visible for E11R and S12G suppressors in conjunction with the PIMs, when compared to the PIMs individually. *In vitro* studies confirm the suppressor containing

mutants refold back to their native conformations, as is evident from the comparable binding affinities to Gyrase, both in the native and refolded states. It was also observed that the M182T substitution in case of the TEM-1 β-lactamase and the N239Y substitution in case of the p53-DBD were able to rescue the folding defect of inactive mutants, largely through thermodynamic and kinetic stabilisation. In addition, several novel suppressors of the SARS-CoV-2 RBD were characterised and shown to stabilise the protein both thermodynamically and kinetically.

Relative to the WT protein, the individual suppressors have a faster refolding rate whereas unfolding rates differ marginally. The ability to refold back faster is consistently observed across all the systems used in this study. This suggests that additional favourable interactions resulting from the mutation are formed prior to the folding transition state, lowering its energy, relative to the unfolded state. In the case of the CcdB S12G, β-lactamase M182T and p53 N329Y mutants, for which crystal structures are available, additional non-covalent interactions present, relative to corresponding WT structure are shown.

The lower flexibility of the loops in the stabilised CcdB mutants S12G, V46L and S60E as compared to WT structure could be one of the reasons for the mutants being more stable than the WT. The difference seen at the 8-12 region for S12G is largely due the series of hydrogen-bonding interactions formed with the G12 and the water molecules, whereas the difference in structure in the 29-46 region in the V46L is largely due to the additional hydrogen-bond interactions formed with the main chain of L46 and R62 and at the 29-46 region in S60E is largely due to the series of salt-bridges formed with the E60 and R48, H55 and R62.

The exact mechanism responsible for E11R suppressor-mediated structural stabilisation cannot be currently assigned due to the unavailability of structures. Comparative analyses of MD simulations performed on the WT and E11R indicate regions of apparent loop stabilisation from residues 41-50 and 85-101 (involved in the C-terminal Gyrase-binding helix), which can possibly account for the global stabilisation of the E11R-containing mutants. In order to probe into the electrostatics of this

charge-reversal stabilising mutation, Tanford-Kirkwood electrostatic calculations have been performed using TKSA-MC server. A significant stabilisation of E11R is observed across a wide pH range from 2 to 12, relative to the WT (data not shown) (52). Electrostatic potential surface maps generated using the UCSF Chimera package show the appearance of a substantial positive - potential surface patch in the loop from residues 8 - 15 harbouring the E11R mutation **(**Figure S1I-J) (53). Thus, it can be speculated that the cluster of positive charges in this loop may prevent the formation of misfolded intermediates during folding of the suppressor.

None of the CcdB suppressor mutations are seen in naturally occurring paralogs. The positions 10, 12 and 46 in CcdB are involved in interactions with one of the ligands- the antitoxin CcdA. The loop from residues 9 to 15 (^{9}KRESRYR^{15}) between the two β-strands contains four residues with their side chains directed towards the CcdA helix. E11 points away from the CcdA helix and mutating it to arginine will abolish the E11- R15 H-bond within the loop and may alter loop conformation. The presence of R10 and S12 in CcdB, in spite of the enhanced stabilities of R10G and S12G proteins, compared to WT, can be explained by the loss of native H-bonds that R10 and S12 make with CcdA, on mutations to glycine. The S60, though not involved directly in CcdA interaction, along with S12 and V46 has been observed to slower down the rejuvenation process of CcdB poisoned Gyrase by CcdA (data not shown).

In the present work, we focus on protein folding kinetics studied in vitro whereas in vivo, for several proteins, folding occurs co-translationally and/or is assisted by molecular chaperones (54). How suppressor mutations affect the kinetics and yield of co-translational or chaperone mediated folding/unfolding is beyond the scope of the present work and it is likely that the different proteins studied make use of different chaperone systems and span both cytoplasmic and periplasmic folding compartments. Nevertheless, it is clear from the present studies that acceleration in folding kinetics *in vitro* is associated with enhanced yield of active protein *in vivo* whether in the context of E. coli or yeast (14,55). A previous study from our laboratory, which looked at the effects of overexpression of

a number of different chaperones on ccdB mutant phenotypes reported the rescue of inactive, folding defective CcdB mutants occurred exclusively in the two *E.coli* strains overexpressing ATP-independent chaperones (SecB and Trigger factor), and not in the strains overexpressing ATP-dependent chaperones that act in the later stages of the folding pathway (9). Till date, there have been reports on the detailed investigation of the Hsp70 and Hsp90-mediated stability and activity of p53 DBD (56–58), the GroEL/ES chaperonin system making transient interactions and inhibiting the folding of β-lactamase precursor (59,60), and of a strongly bound complex of the GroEL chaperone with the receptor-binding domain of the SARS CoV2 spike protein (61). However, none of these discuss the effects of suppressor mutations on chaperone mediated folding kinetics.

We have summarized the effect of the suppressor mutations characterized in the present study on various kinetic parameters in the background of both WT and inactive mutants (Table 1). For the PIM/Suppressor pair analysis, we excluded the p53DBD double mutants since we did not have the corresponding inactive mutants for comparison. We observe that except for one suppressor which has a similar rate constant as the WT for the slow phase of refolding and one PIM-suppressor pair which had a similar burst phase of refolding as compared to the inactive mutant, all other suppressors or PIM-suppressor pairs have an effect on both the refolding and unfolding kinetic parameters. To further delineate the parameters which are most effected by the suppressor mutations we calculate the average fold change of each parameter by the suppressor mutations (Table 1) as follows:

$P_{avg} = \frac{\sum_1^n \boldsymbol{Pi}}{\boldsymbol{n}}$,……..equation 1

where P_{avg} is the average fold change of a parameter P,

P_i is the fold change of that parameter in the background of the suppressor which is = $P_i = P_{supp}/P_{wt}$, or

$P_i = P_{(inactive,\ suppressor)}/P_{inactive}$

and n is the number of mutants. A non-parametric Mann Whitney test is performed to show that the mean of the distributions of each of these values of P_i is significantly higher (or lower) than 1 (Figure 8B-C).

Values of P_i are summarized in Table 1. and confirm that the effect of the suppressor mutants is statistically significant for the refolding rates in background of both WT and inactive mutations.

In summary, the present study showed that the suppressors are able to achieve high kinetic and thermodynamic stability even in the background of a stable WT protein such as CcdB (T_m= 66 °C) (Figure 8) and glycosylated and secreted proteins such as a potential COVID-19 vaccine candidate. Further, the effects of suppressors were primarily on the refolding rate parameters. This was observed across multiple suppressors in multiple proteins, suggesting this to be the primary mechanism through which such suppressors function.

Conclusions

The data presented here consistently shows that the global suppressors result in a small amount of stabilization of the wild-type protein but greatly enhance the foldability of folding defective, loss of function mutants, primarily through an increase in the refolding rate constants and burst phase amplitude. Suppressors promote increased *in-vivo* solubility and yield, as well as regain-of-function phenotypes. These observations hold true across these diverse protein systems with proteins from both prokaryotes and eukaryotes, including both cytoplasmic and secreted proteins, suggesting these are general results. The results also show that such mutations cannot be easily predicted by existing computational predictors of protein stability effects, and thus genetic screens remain essential to isolate such mutants. The study also demonstrates that the global suppressor approach can be used to consistently stabilise wild-type proteins, including ones for therapeutic and vaccine applications and highlights the importance of such suppressor screening to create molecules that are both thermodynamically and kinetically stable to unfolding and aggregation. Results presented here clearly

demonstrate that the primary mechanism by which global suppressors function is by increasing refolding rates and also suggest that mutational effects on folding kinetics rather than thermodynamic stability are important *in vivo*.

Materials and Methods

Plasmids and Host Strains

CcdB: The ccdB gene was cloned under the control of P_{BAD} promoter in pBAD24 vector (11). Two *Escherichia coli* host strains *Top10*pJAT and *Top10GyrA* were used. *Top10*pJAT is a CcdB sensitive strain and was used for screening the phenotypes. The pJAT8araE plasmid which encodes for the arabinose transporter area was introduced into the *TOP10* strains to ensure that in all cells there is approximately equal amounts of arabinose uptake (62). *Top10GyrA* is resistant to the action of CcdB toxin and was used for monitoring the expression of mutant proteins. The strain contains a GyrA462 mutation in its genome that prevents CcdB from binding to Gyrase (10).

TEM-1 and p53-DBD: WT and mutant TEM-1 β lactamase with a C-terminal 6xHistidine tag were cloned and expressed under the control of the T7 promoter in the pET-24a vector. The native signal sequence was used for efficient secretion in the *Escherichia coli* host strain BL21 (DE3) pLysE. WT and mutant p53-DBD genes with N-terminal 6xHistidine tag were cloned and expressed under the control of the T7 promoter in the pET-15b vector. *Escherichia coli* host strain BL21 Rosetta (DE3) was used for expressing the p53-DBD proteins.

mRBD: mRBD WT and mutants were expressed from mammalian cell culture as described previously (33) under the control of the CMV promoter along with a tPA signal sequence for efficient secretion.

Mutagenesis

CcdB: For single mutants V5F, Y8D, E11R, S12G, V18W, V20F, L36A, V46L, S60E and L83S, as well as for double mutants, V18W-E11R, V20F-E11R, L36A-E11R and L83S-E11R, the ccdB gene was amplified in two fragments with the desired point mutations. The fragments had overlapping

regions (introduced during PCR) of 15-20 nucleotides, which were then recombined using Gibson assembly. Amplification was done using Phusion Polymerase from NEB as per the manufacturer's protocol. The double mutants V5F-S12G, V18W-S12G, V20F-S12G, L36A-S12G and L83S-S12G were synthesized by GeneArt (Germany).

TEM-1 and p53-DBD: The TEM-1 β lactamase WT and mutants M182T, M69I, M69I-M182T, L76N, L76N-M182T and p53-DBD WT and mutants N239Y, V143A, V157F, V143A-N239Y, V157F-N239Y were synthesized by GenScript (USA).

mRBD (331-532): The mRBD (331-532) codon optimised for human cell expression was synthesized by GenScript (USA) (33). For single mutants D389E, L390M and P527I, the RBD gene was amplified in two fragments with the desired point mutations. The fragments had overlapping regions (introduced during PCR) of 15-20 nucleotides, which were then recombined using Gibson assembly. Amplification was done using Phusion Polymerase from NEB as per the manufacturer's protocol.

Protein expression and purification

CcdB: WT CcdB and all mutants were expressed from the arabinose promoter P_{BAD} in the pBAD24 vector in the CcdB resistant Top10Gyrase strain of *E. coli*. The purification of the CcdB mutants were carried out as described previously (17). Briefly, 500 mL of LB medium (HiMedia) was inoculated with 1% of the primary inoculum and grown at 37 °C until the OD_{600} reached 0.6. Cells were then induced with 0.2% (w/v) arabinose and grown at 37 °C for 5 hours for WT CcdB, Y8D, E11R, S12G, V46L, S60E and the double mutants V18W-S12G, V20F-S12G, L36A-S12G and L83S-S12G, at 25 °C overnight for the inactive mutants V18W, V20F, L36A and L83S and at 20 °C overnight for the double mutants L36A-E11R and L83S-E11R. Cells were harvested, re-suspended in HEG re-suspension buffer pH 7.4 (10 mM HEPES, 50 mM EDTA, 10% glycerol containing 10 mM PMSF) and lysed by sonication. The supernatant was incubated with Affi-gel15 (Biorad) coupled to CcdA peptide (residues 46-72) and incubated overnight at 4 °C. The unbound fraction was removed and

washed with five times the bed volume of coupling buffer pH 8.3 (0.05 M Sodium Bicarbonate, 0.5 M Sodium Chloride). The elutions were carried out with 0.2 M Glycine, pH 2.5 into a tube containing an equal volume of 400 mM HEPES, pH 8.4, 4 °C (9,17). The eluted fractions were subjected to 15% Tricine SDS-PAGE and the protein concentration was determined. Fractions containing pure protein were pooled and stored at −80 °C.

TEM-1 β lactamase: The TEM-1 β lactamase mutants were purified as described previously (22) with slight modifications. The recombinant BL-21 (λDE3, plysE) strains were grown in TB medium at 37 °C containing 50 μg/mL kanamycin until the OD_{600} reached 0.8 and protein expression was induced by addition of 1.0 mM IPTG. The induced cultures were grown overnight with shaking at 30 °C and were harvested by centrifugation. The periplasmic fraction was obtained by osmotic shock by resuspending first in lysis buffer, pH 7.0 (10 mM HEPES, 0.5 mM EDTA, 20% sucrose, 0.05% SDS, lysozyme and protease inhibitor) at 37 °C with shaking for 1 hr, followed by addition of an equal volume of ice cold milliQ water, incubated at 4 °C for an hour, followed by addition of 100 μL of 2 M $MgCl_2$. The clarified lysates were loaded on 2 ml of Q-Sepharose fast flow (Amersham Biosciences, Uppsala, Sweden). The elutes obtained by a gradient of 100-500mM NaCl in 10 mM HEPES, 10% glycerol pH 7.0, were further subjected to Ni-NTA purification by mixing with 2 mL of Ni-Sepharose resin (GE Healthcare) for 4 hrs and the bound proteins were eluted with a gradient of 100-500 mM imidazole in 10 mM HEPES, 300 mM NaCl, 10% glycerol (pH 7.0). The purified proteins were subjected to 15% Tricine SDS-PAGE, concentrated, buffer exchanged to remove imidazole, and finally stored in storage buffer (10 mM HEPES, 300 mM NaCl, 10% glycerol, pH 7.0) at -80 °C until further use. Yield for all mutants varied from 0.5-10 mg/L.

p53-DBD: The p53-DBD mutants were purified as described previously (63) with slight modifications. The recombinant BL-21 Rosetta (DE3) strains were grown in TB medium at 37 °C containing 100 μg/mL ampicillin until the OD_{600} reached 1.0. 100 μM $ZnSO_4$ was added and incubated at 25 °C for 30 mins. Protein expression was induced by addition of 1.0 mM IPTG. The induced

cultures were grown for 20 hours with shaking at 25 °C and were harvested by centrifugation. Cells were harvested, re-suspended in lysis buffer pH 7.2 (50 mM NaH_2PO_4, 100 mM NaCl, containing 10 mM PMSF and 10 mM DTT) and lysed by sonication. The clarified lysates were loaded first with 2 ml of DEAE Sepharose fast flow (GE Healthcare) and the elutes obtained by a gradient of 100-500 mM NaCl in 50 mM NaH_2PO_4, pH 7.2, were further subjected to Ni-NTA purification by mixing with 2 mL of Ni-Sepharose resin (GE Healthcare) for 4 hrs. The bound proteins were eluted with a gradient of 100-500 mM imidazole in 50 mM NaH_2PO_4, 500 mM NaCl, (pH 7.2) containing 10 mM DTT. The purified proteins were subjected to 15% Tricine SDS-PAGE, concentrated and finally stored in storage buffer (50 mM NaH_2PO_4, 500 mM NaCl, 500 mM imidazole, 10 mM DTT, pH 7.2) at -80 °C until further use. The inactive mutants V143A, V157F, could not be used for biophysical studies because of their low expression, solubility, poor yields and high tendencies towards aggregation after purification. Yield for the wild type and the mutants varied from 0.5-2 mg/L.

mRBD (331-532): Expression and purification of the mRBD and the single mutants D389E, L390M and P527I was carried out as described previously (33). Briefly, proteins were expressed by transient transfection of Expi293 cells and purified by Ni-NTA chromatography. The eluted fractions were pooled and dialysed thrice using a 3-5 kDa (MWCO) dialysis membrane (40mm flat width) (Spectrum Labs) against 1XPBS, pH 7.4 (storage buffer). The eluted fractions were subjected to 15% Tricine SDS-PAGE and the protein concentration was determine by measuring the A_{280} and using an extinction coefficient of 33850 $M^{-1}cm^{-1}$.

***In vivo* activity of the different CcdB mutants**

Wild type and mutant CcdB were transformed into *E.coli Top10*pJAT, grown for 1 hour in 1 ml LB media containing 0.2% glucose (highest repressor level to avoid leaky expression). After 1 hour, the cells were pelleted and glucose was removed by subjecting cells to three washes with 1 ml LB. Finally, equal amounts of cells resuspended in 1 ml of LB media and serially diluted were spotted on seven agar plates (LB agar plates containing 100 µg/mL ampicillin, 20 µg/mL gentamycin) containing

various amounts (%) of glucose (repressor) and arabinose (inducer) concentrations (i.e. 2×10^{-1} % glu, 4×10^{-2} %glu, 7×10^{-3} % glu, 0% glu/ara, 2×10^{-5}% ara, 7×10^{-5}% ara and 2×10^{-2} % ara) at 37 ˚C. Since active CcdB protein kills the cells, colonies are obtained only for mutants that show an inactive phenotype under the above conditions (9).

***In vivo* Solubility Estimation**

CcdB: Solubility levels were monitored for all the single and double mutants in *E. coli Top10Gyrase* in the presence of 0.2% arabinose as described previously (9). Cultures were grown in LB media, induced with 0.2% arabinose at an OD_{600} of 0.6 and grown for 5 hours at 37 °C. 2×10^{9} cells were centrifuged (1800g, 10 min, RT). The pellet was resuspended in 500 µL HEG buffer pH 7.4 (10 mM HEPES, 50 mM EDTA, 10% glycerol containing 10 mM PMSF) and sonicated. 250 µL was taken as Total Cell Lysate and the remaining 250 µL was centrifuged (11000 g, 10 min, 4 °C). 250 µL was taken as supernatant and the pellet was resuspended in 250 µL HEG buffer pH 8.4 and all the fractions were subjected to 15% Tricine SDS-PAGE. Solubility of all mutants was quantitated by estimating relative amounts of CcdB in supernatant and pellet fractions by the geldoc software (Quantity One) (9,64).

p53 DBD: Solubility levels were monitored for all the single and double mutants in *E. coli* BL-21 Rosetta (DE3) cells. Cultures were grown in LB media till they attain OD_{600} values of 1.0, followed by incubation with 100 µM $ZnSO_4$ at 25 °C for 30 minutes and induction with 1.0 mM IPTG, for 20 hours at 25 °C. 2×10^{9} cells were centrifuged (1800g, 10 min, RT) and the pellet was resuspended in 500 µL lysis buffer pH 7.2 (50 mM NaH_2PO_4, 100 mM NaCl, containing 1 mM PMSF and 10 mM DTT) and sonicated. 250 µL was taken as Total Cell Lysate and the remaining 250 µL was centrifuged (11000 g, 10 min, 4 °C). 250 µL was taken as supernatant and the pellet was resuspended in 250 µL lysis buffer pH 7.2 and all the fractions were subjected to 15% Tricine SDS-PAGE. Solubility of all

mutants was quantitated by estimating relative amounts of the p53 DBD protein in supernatant and pellet fractions by the geldoc software (Quantity One) (9,64).

Thermal stability measurements by TSA and nanoDSF

CcdB: The thermal shift assay was conducted in an iCycle Q5 Real Time Detection System (Bio-Rad, Hercules, CA) using 4 µM of the CcdB protein in 200 mM HEPES, pH 8.4 and 2.5X Sypro orange dye in a 96-well iCycleiQPCR plate. The plate was heated from 20 to 90 °C. with a ramp of 0.5 °C/min. The fluorescence data following CCD detection was plotted as a function of temperature and fitted to a standard, four parameter sigmoidal equation $y= LL+\{UL-LL\}/\{1+exp((T_m-T)/a)\}$, where y is the observed fluorescence signal, LL and UL are the minimum and maximum intensities in the transition region respectively, 'a' is the slope of the transition, T_m is the melting temperature, and T is the experimental temperature (15).

nanoDSF (Prometheus NT.48) was also used to carry out thermal unfolding experiments of the CcdB mutants. The assays were carried out with 4 µM of each protein and the apparent thermal stability (T_m) was determined by monitoring the changes in the fluorescence ratio (F350/F330) as a function of temperature as described earlier (17). A subset of the CcdB mutants were also refolded in 1.5 M GdnCl and subjected to thermal denaturation with native protein in 1.5 M GdnCl as a control. For thermal denaturation, the samples were filled into capillaries and then placed the instrument. The capillaries were then heated from 20 to 90 °C with a ramp of 1 °C /min. For the highly stable mutants Y8D, V46L and S60E as well as WT, refolding was carried out in 1, 2, 3, 4 and 5 M GdnCl and refolded protein subjected to thermal denaturation. Native protein in 1, 2, 3, 4 and 5 M GdnCl was also taken as control.

TEM-1 β lactamase, p53-DBD, and mRBD (331-532): nanoDSF (Prometheus NT.48) was also used to probe the thermal unfolding of the TEM-1 β lactamase, p53-DBD and mRBD mutants. The assays were carried out with 4 µM of each protein and the apparent thermal stability (T_m) was determined by monitoring the changes in the fluorescence ratio (F350/F330) as a function of temperature. Samples

were heated from 20 to 90 °C with a ramp of 1 °C /min. TEM-1 β lactamase and p53 DBD were refolded in 0.5 M GdnCl and 0.5 M urea respectively and subjected to thermal denaturation along with the native proteins in 0.5 M GdnCl and 0.5 M urea as their respective controls. For the highly stable mRBD mutants D389E, L390M and P527I as well as WT, refolding was carried out in 0.5, 1, 2, and 3 M GdnCl and refolded protein subjected to thermal denaturation with native protein in 0.5, 1, 2, and 3 M GdnCl as controls.

Isothermal denaturation

CcdB: Equilibrium unfolding experiments of the CcdB mutants were carried out by nanoDSF (Prometheus NT.48) as described previously (17). Briefly, all the CcdB mutant proteins were overnight dialysed four times in total of 2 litres of 200 mM HEPES, pH 8.4 using Tube-O-Dialyser (4kDa MWCO, GBiosciences). The chemical stability (C_m) was then determined using 5 µM of proteins by monitoring the changes in the fluorescence ratio (F350/F330), after overnight incubation at 25 °C containing various concentrations of the denaturant (GdnCl). The GdnCl concentrations were estimated from refractive index measurements using a refractometer. The data was analyzed using Sigmaplot™ for Windows™ scientific graphing software, and the plots were fitted to a two-state unfolding model ($N_2 \leftrightarrow 2U$). The fraction unfolded for all CcdB mutants was calculated as described (11,17) and is summarized below.

The spectroscopic signal (Y) of a protein solution (F_{350}/F_{330} ratio by nano-DSF) is related to the fraction of unfolded protein (f_u) by:

$$f_u = (Y - Y_f)/(Y_u - Y_f) \quad (1)$$

where Y_f and Y_u are the values of Y for the folded and unfolded protein respectively. These change linearly with the denaturant concentration ([D]), as follows:

$$Y_f = y_f + m_f[D] \quad (2)$$

$$Y_u = y_u + m_u[D] \quad (3)$$

where y_f and y_u are the folded and unfolded parameters at zero denaturant concentration. m_f and m_u are the denaturation dependence of Y for the folded and unfolded state respectively.

TEM-1 β lactamase, p53-DBD and mRBD (331-532): Equilibrium unfolding experiments of the monomeric TEM-1 β lactamase, p53-DBD and mRBD mutants were also carried out by nanoDSF (Prometheus NT.48). The stability to chemical denaturation (C_m) was determined by monitoring the changes in the fluorescence ratio (F350/F330), after overnight incubation at 25 °C in the final storage buffer for TEM-1 and mRBD mutants containing various concentrations of the denaturant (GdnCl) and overnight incubation at 15 °C in the final storage buffer for p53-DBD mutants containing various concentrations of the denaturant (Urea). The data was analyzed using Sigmaplot™ for Windows™ scientific graphing software, and the data were fit to a two-state unfolding model (N↔U) for TEM-1 β lactamase and p53-DBD mutants and a three-state unfolding model (N↔I↔U) for the mRBD mutants. Isothermal denaturation was carried out at a fixed protein concentration of 5 µM for all the proteins. The fraction unfolded for all the TEM-1 β lactamase, p53-DBD and mRBD mutants were calculated in a similar way as described above.

Refolding and unfolding kinetics

CcdB: Refolding and unfolding kinetics for all the mutants were monitored by nanoDSF using PR.Time Control software (Prometheus NT.48) at 25 °C, pH 8.4 as described previously (17). Briefly, the refolding rates were measured using different concentrations (1 µM -5 µM) of the dialysed proteins in 200 mM HEPES, pH 8.4 denatured in 0.2-4 M GdnCl and subsequently diluted to final denaturant concentrations varying from 0.1 M to 1.5 M of GdnCl, and the changes in the fluorescence ratio (F350/F330) were monitored as a function of time. To measure the unfolding kinetics, protein in native buffer (200 mM HEPES, pH 8.4) was diluted into the same buffer containing 8 M GdnCl to a final concentration of GdnCl varying from 2 to 4 M and the changes in the fluorescence ratio (F350/F330) were monitored as a function of time. Refolding kinetic traces of fluorescence intensity from 0.1 M to 1.5 M GdnCl as a function of time for different CcdB mutants were normalized from 0 to 1 between

native and denatured baseline, as described previously (9,16,17). Unfolding kinetic traces of fluorescence intensity from 2 to 4 M GdnCl as a function of time for different CcdB mutants in 200 mM HEPES, pH 8.4 were normalized from 0 to 1 between native and denatured baseline, as described previously (16,17). For the stable CcdB mutants (Y8D, V46L and S60E as well as WT CcdB) refolding and unfolding was carried out in 2 M and 4.5 M GdnCl respectively in 200 mM HEPES, pH 8.4 at 25 °C and normalisation was done as described above. The data was analyzed using Sigmaplot™ for Windows™ scientific graphing software and plots were fitted to a 5 parameter equation for exponential decay for refolding ($y=a_0+a1*\exp(-kf_1*x)+a2*\exp(-kf_2*x)$), and a 3 parameter exponential rise for unfolding ($y=A_0+A1*(1-\exp(-ku_1*x))$) as described previously (16), where x is the time of refolding/unfolding. Both refolding and unfolding studies of all the mutants were also carried out at three different denaturant concentration and the observed rates were plotted as a function of denaturant condition to determine the refolding and unfolding m values (M^{-1}). This was further used to extrapolate the unfolding and refolding rates of all the mutants to 0 M GdnCl concentration for relative comparison.

TEM-1 β lactamase, p53-DBD and mRBD (331-532): Refolding and unfolding kinetics of the TEM-1 β lactamase and mRBD mutants at 25 °C and of the p53-DBD mutants at 15 °C were also monitored by nanoDSF using PR.Time Control software (Prometheus NT.48). Briefly, the refolding rates for the TEM-1 β lactamase and the mRBD mutants were measured using 5 µM of the proteins denatured in storage buffer containing 3 M GdnCl and subsequently diluted to a final concentration of 0.5 M of GdnCl, and the changes in the fluorescence ratio (F350/F330) were monitored as a function of time. For the p53 DBD mutants, the refolding rates were measured using 4 µM of the proteins denatured in the final storage buffer containing 4 M urea and subsequently diluted to a final concentration of 2 M urea.

To measure the unfolding kinetics, protein in native storage buffer was diluted into buffer containing 2.5 M GdnCl for TEM-1 β lactamase and 3 M GdnCl for mRBD mutants and 4.4 M Urea for p53-

DBD and the changes in the fluorescence ratio (F350/F330) were monitored as a function of time. Refolding and unfolding kinetic traces were normalized from 0 to 1 between native and denatured baselines. The data for the TEM-1 β lactamase mutants was analyzed using Sigmaplot™ for Windows™ scientific graphing software and plots were fitted to a 5 parameter equation for exponential decay for refolding ($y=a_0+a1*exp(-kf_1*x)+a2*exp(-kf_2*x)$), yielding slow and fast phase rate constants and a 3 parameter exponential rise for unfolding ($y=A_0+A1*(1-exp(-ku_1*x))$) as described above, where x is the time of refolding/unfolding. The data for the mRBD mutants was analyzed using Sigmaplot™ for Windows™ scientific graphing software and plots were fitted to a 3 parameter equation for exponential decay for refolding ($y=a_0+a1*exp(-kf_1*x)$), and a 5 parameter exponential rise for unfolding ($y=A_0+A1*(1-exp(-ku_1*x))+a2*(1-exp(-ku_2*x))$), yielding slow and fast phase rate constants as described above, where x is the time of refolding/unfolding. The data for the p53 DBD mutants was analyzed using Sigmaplot™ for Windows™ scientific graphing software and plots were fitted to a 5 parameter equation for exponential decay for refolding ($y=a_0+a1*exp(-kf_1*x)+a2*exp(-kf_2*x)$), yielding slow and fast phase rate constants and a 5 parameter equation for exponential rise for unfolding ($y=A_0+A1*(1-exp(-ku_1*x))+a2*(1-exp(-ku_2*x))$), yielding slow and fast phase rate constants as described above, where x is the time of refolding or unfolding.

Binding of native and refolded CcdB proteins to Gyrase A-14 by MicroScale Thermophoresis (MST)

6.6 µM GyraseA-14 (in 1X PBS) was labeled using the RED-NHS Monolith™ Protein Labeling Kit (NanoTemper Technologies) according to the manufacturer's instructions. After labeling, the protein was eluted by gravity flow using a PD MiniTrap™ G-25 (GE Healthcare) Sephadex column into 200 mM HEPES, pH 8.4 which was also used as assay buffer for MST experiments. Labeled Gyrase-A14 was used as target at a concentration of 70 nM, while non-fluorescent CcdB proteins were titrated in a 1:1 dilution series (highest concentrations range between 100 nM and 10 µM). The binding of labeled Gyrase to refolded CcdB mutants in 1.5 M GdnCl (also in 0.1 M GdnCl for V18W, V18W-S12G,

V20F and V20F-S12G) as well as native CcdB proteins, not subjected to refolding, in presence of 1.5 M GdnCl (also in 0.1 M GdnCl for V18W, V18W-S12G, V20F and V20F-S12G) was measured. Samples were loaded into Monolith™ NT.115 MST Standard Capillaries (NanoTemper Technologies) and binding measured using a Monolith NT.115 instrument with MO.Control software at room temperature (LED/excitation power setting 100%, MST power setting 80-100%). Data was analyzed using MO.Affinity Analysis software (version 2.2.5, NanoTemper Technologies) at different standard MST-off times.

Affinity and thermal tolerance of the CcdB proteins measured by Surface Plasmon Resonance (SPR)

All SPR experiments were performed with a Biacore 2000 (Biacore, Uppsala, Sweden) optical biosensor at 25 °C. 35 µg/mL of Gyrase was used for immobilization at 30 µl/min flow rate for 180 s. 1000 resonance units of Gyrase were attached by standard amine coupling to the surface of a research-grade CM5 chip. A sensor surface (without Gyrase) that had been activated and deactivated served as a negative control for each binding interaction. The E11R CcdB mutant proteins (E11R, L36A-E11R and L83S-E11R) were overnight dialysed three times against a total 6 litres of 1XPBS, pH 7.4 using Tube-O-Dialyser (4 kDa MWCO, GBiosciences). The remaining proteins were in 200 mM HEPES-0.1 M glycine, pH 8.4. Different concentrations of the dialysed CcdB mutants were run across each sensor surface in a running buffer of PBS (pH 7.4) containing 0.005% Tween surfactant. Protein concentrations ranged from 3 nM to 5 µM. Both association and dissociation were measured at a flow rate of 30 µl/min. In all cases, the sensor surface was regenerated between binding reactions by one to two washes with 4 M $MgCl_2$ for 10 –30 s at 30 µL/min. Each binding curve was corrected for nonspecific binding by subtraction of the signal obtained from the negative control flow cell. The kinetic parameters were obtained by fitting the data to a simple 1:1 Langmuir interaction model by using BIA EVALUATION 3.1 software as described previously (9,65). Thermal tolerance of the CcdB mutants E11R, S12G, L36A, L36A-E11R and L36A-S12G and WT CcdB using 500 nM of protein

was assessed by their ability to bind GyraseA-14 after heat stress. The protein sample was incubated at 40 °C and 80 °C respectively for 1 h in a PCR cycler (BioRad) with a heated lid to prevent evaporation. The samples were cooled to 25 °C and binding affinity to Gyrase was determined by SPR experiments as described above The fraction of active protein following thermal stress was quantitated by measuring the RUs at the end of the association time period relative to those for the same protein incubated throughout at 25 °C. This was designated as Residual activity.

Molecular dynamics simulations

The starting structures for the simulation were 3VUB for WT and the solved structure S12G for the mutant. For the other three mutants E11R, L36A, L36A-S12G, the structure was modelled and then simulated. Before proceeding for simulation, waters were removed from the structure but chloride ions were retained, residues with multiple occupancies were edited to include the conformation with the highest occupancy and any missing side chains were modelled using Coot. In all cases, the dimeric structures were used and were generated by selecting the suitable symmetry equivalent molecule. Simulations were carried out using Gromacs version 2019.2 (66) with OPLSAA forcefield (67). Structures were enclosed in a dodecahedral simulation box in which the distance between the protein and the box was set to 1.2 nm. The box was solvated using a TIP4P (68) water model, protein inside the box was used with standard protonation states and charges of the system were neutralized using Na^+ or Cl^- ions. The PME or particle mesh Ewald (69) was used for treating electrostatics. A distance cut off for Coulombic interaction was 1.0 nm, a Fourier spacing of 0.16 nm with a fourth degree interpolation, while van der waal's cut off was set to 1 nm. In order to remove any short contacts, energy minimization was carried our using a conjugate gradient method and with 1 kJ mol^{-1} nm^{-1} as the maximum force before the minimization converges. The minimized structure was subjected to temperature equilibration (NVT) at temperatures of either 293 K or 313 K using Nośe-Hoover (70,71) thermostat with a coupling time constant τ_T of 0.4 ps. The protein and non-protein atoms were separately coupled to the temperature baths. Initial velocities at appropriate temperatures were

generated using a Maxwell-Boltzmann distribution. The structure after temperature equilibrium was further pressure (NPT) equilibrated for another 100 ps using the Parinello-Rahman barostat (72) with a coupling time constant τ_p of 2 ps. A position restrained dynamics of 100 ps was run for both NVT and NPT equilibration with a force constant of 1000 kJ mol^{-1} nm^{-2} on each protein atom. After removing the restraints, the production MD was run for 50 ns (27 ns for 4VUB) with a time step of 2 fs. The velocity, trajectory and energy were saved at every 2 ps.

MIC and IC_{90} determination of TEM-1 β lactamase mutants: MIC and IC_{90} were calculated as described previously (22). Briefly, *E. coli* BL-21 (λDE3, plysE) was used as the host strain for determining the ampicillin and cefotaxime MIC of the pET24a-TEM-1-WT, M182T, M69I, M69I-M182T, L76N, L76N-M182T constructs. Cultures were grown overnight at 37 °C in LB broth with 50 μg/mL kanamycin. . The overnight cultures were diluted 1:10^4 and 30 μL was inoculated into 500 μL of fresh LB broth supplemented with 50 μg/mL kanamycin, 100 μM IPTG inducer, and various concentrations of ampicillin and cefotaxime. The concentrations of ampicillin used for MIC determination were 0, 25, 50, 100, 200, 300, 400, 500, 600, 800, 1000, 1500, 2000, 2500, 3000 and 4000 μg/mL. The concentrations of cefotaxime tested were 0, 1, 2, 3, 4, 5, 6, 8, 10, 15, 20 and 30 μg/mL. The cultures were then incubated at 37 °C with shaking for 24 hrs following which OD_{600} measurements were carried out on Varioskan Flash (ThermoScientific) using Nunclon delta surface plates (ThermoScientific). and the MIC was determined by recording the lowest concentration of ampicillin or cefotaxime on which no growth was observed. In practice, this was an all or none phenomenon (24).

IC_{90} was derived directly from the plate data measurements. Briefly, *E. coli* BL-21 (λDE3, plysE) containing the pET24a plasmid that encodes TEM-1 β-lactamase mutants was grown overnight in LB broth with 50 μg/mL kanamycin. Overnight cultures were diluted 1:100 into LB broth with 50 μg/mL kanamycin and incubated for 4 hrs at 37 °C to mid-log phase (OD_{600} ~0.6). Ten-fold serial dilutions of

each culture were made, and 100 μL of each dilution was spread onto LB agar plates containing 100 μM IPTG inducer and 0-4000 μg/mL ampicillin and 0-50 μg/mL of cefotaxime, in a series of two-fold increases. After incubation for 24 hrs at 37 °C, colony forming units (cfu) on each plate were counted to calculate the cfu/mL of culture, and IC_{90} was defined as the concentration of ampicillin or cefotaxime that reduces cfu/mL of culture by ≥90% (22).

Nitrocefin assay of TEM-1 β lactamase mutants: TEM-1 β -lactamase activity was assayed as described previously (7). Briefly the rate of nitrocefin (50 μM) hydrolysis was observed at 486 nm at 25 °C for 60 minutes in 10 mM HEPES, 300 mM NaCl, 10% glycerol (pH 7.0) using10 nM native protein, native protein in 0.5 M GdnCl and refolded protein in 0.5 M GdnCl. Activity measurements were carried out on Varioskan Flash (ThermoScientific) using Nunclon delta surface plates (ThermoScientific).

SPR-binding of native, native in presence of GdnCl and refolded mRBD proteins with immobilized ACE2-hFc: Binding studies of various mRBD mutants with ACE2-hFc neutralizing antibody were carried out using the ProteOn XPR36 Protein Interaction Array V.3.1 from Bio-Rad as described previously (33). Briefly, following activation of the GLM sensor chip with EDC and sulfo-NHS (Sigma), Protein G (Sigma) was coupled at 10 μg/mL in the presence of 10 mM sodium acetate buffer pH 4.5 at 30 μL/min for 300 seconds until ~3500-4000 RU was immobilized. After quenching the excess sulfo-NHS esters using 1 M ethanolamine, ~1000 RU of ACE2-hFc was immobilized at a flow rate of 5 μg/mL for 100 seconds on various channels except one blank channel that served as the reference channel. Native mRBD proteins, proteins in 0.5 M GdnCl and refolded protein in 0.5 M GdnCl were passed at a flow rate of 30 μL/min for 200 seconds over the chip surface, followed by a dissociation step of 400 seconds. A lane without any immobilization was used to monitor non-specific binding. After each kinetic assay, the chip was regenerated in 0.1 M Glycine-HCl (pH 2.7). 50 nM of the mRBD proteins in 1X PBS were used in all cases for the binding studies. The response units for

each of the native protein, native protein in 0.5 M GdnCl and refolded proteins in 0.5 M GdnCl was used for relative comparisons. For the studies carried out in GdnCl, the running buffer did not have any GdnCl and the jumps obtained in all the channels were removed after reference subtraction.

Crystallization of CcdB mutants

The purified mutants of CcdB, S12G, V46L and S60E CcdB, in 1xPBS pH 7.4 and 1 mM EDTA at a concentration of 5 mg/ml was screened for crystallization with Hampton Research screens by the sitting drop method using the Mosquito crystallization robot facility at NCBS/Instem. Plates were incubated at 18 °C. Crystals appeared in a few conditions after approximately 20 days. Two conditions had mountable crystals: 0.2 M calcium chloride dihydrate, 20% w/v PEG 3350, pH 5.1 (PEG/Ion 1, condition 7) and 0.2 M ammonium chloride, 20% w/v PEG 3350, pH 6.3 (PEG/Ion 1, condition 9). The initial crystals diffracted to ~2.5 Å. Conditions were further optimized to obtain single crystals for better diffraction quality. The best crystals were obtained in the condition 0.15 M calcium chloride dihydrate, 20% w/v PEG 3350 for S12G; 0.20 M calcium chloride dihydrate, 25% w/v PEG 3350, pH 5.1 with 20% glycerol (cryo) for V46L; 0.20 M calcium chloride dihydrate, 10% w/v PEG 3350; pH 5.1 with 20% glycerol (cryo) for S60E, with a protein:precipitant ratio of 1:2 at 18 °C using the hanging drop method.

Data collection and processing of CcdB mutants

Diffraction data was collected at 100K using Rigaku FR-X with R-AXIS IV++ detector facility at NCBS/Instem for S12G. For V46L, diffraction data was collected at 100K using XRD2 beamline with Dectris Pilatus-6M detector facility at Elettra synchrotron, Trieste, Italy. For S60E, diffraction data was collected at 100K using Rigaku MicroMax-007HF with mar345dtb detector facility at home-source MBU, IISc. The crystals diffracted to 1.63Å, 1.35 Å and 1.93 Å for S12G, V46L and S60E respectively. Data was processed using iMosflm (73,74) with an overall completeness of 90.6% for S12G, 100% for V46L and 97.5% for S60E. For S12G, the crystal belonged to the C2 space group,

with the unit cell parameters, while the pointless predicted I2. Thus, the data was re-scaled in I2 with unit cell parameters a = 35.57; b = 36.53; c = 67.53 and β = 93.69°. The V46L and S60E crystals belonged to the C2 space group with unit cell parameters a = 75.10; b = 36.76; c = 35.91 and β = 115.19° for V46L and a = 74.81; b = 36.64; c = 35.67 and β = 114.97° for S60E. The structure was solved by molecular replacement using PHASER (75) with 3VUB (76) as the starting model. After iterative cycles of refinement using Refmac (77,78) and manual model building using Coot (79,80), the final model consisted of 816 protein atoms, 95 water and two Cl^- ion with an R_{factor} and R_{free} of 22.8 and 26.9 respectively for S12G. For V46L, the final model consisted of 814 protein atoms, 167 water and two Cl^- ion with an R_{factor} and R_{free} of 16.2 and 18.4 respectively. For S60E, the final model consisted of 820 protein atoms, 98 water and two Cl^- ion with an R_{factor} and R_{free} of 17.0 and 21.4 respectively. Composite omit maps were calculated around the 12th, 46th and 60th residue for S12G and S60E respectively. The final model was validated using the validation server (https://validate.wwpdb.org). Data processing and refinement statistics are given in Supplementary Table S10. The server "https://swift.cmbi.umcn.nl/servers/html/listavb.html" was used for calculating the average B-factors.

Declarations:

Conflict of interest statement: None.

Ethics Approval and consent to participate: Not Applicable.

Consent for publication: Not Applicable.

Data availability: The crystal structures of the CcdB mutants have been deposited in PDB with PDB IDs: 7EPG (CcdB S12G), 7EPJ (CcdB V46L) and 7EPI (CcdB S60E). The validation reports of the structures are submitted along with the manuscript. The structures will be available after publication. The data relevant to the figures in the paper have been made available within the article and in the supplementary information section. Further information and requests for resources and reagents should be directed to and will be fulfilled by the Lead Contact, Prof. Raghavan Varadarajan (varadar@iisc.ac.in). Lead contact for the material availability: Prof. Raghavan Varadarajan (varadar@iisc.ac.in). All unique/stable reagents generated in this study are available from the Lead Contact without restriction.

Competing interests: None.

Funding: This work was funded in part by a grant to RV from the Department of Biotechnology, grant number-BT/COE/34/SP15219/2015, DT.20/11/2015), Government of India and supported by National Institutes of Health Grant R01A1118366-01. We also acknowledge funding for infrastructural support from the following programs of the Government of India: DST FIST, UGC Centre for Advanced study, Ministry of Human Resource Development (MHRD), and the DBT IISc Partnership Program. The NCBS X-ray Facility was supported by Grant BT/PR5081/INF/156/2012 from the DBT. The MBU, IISc X-ray Facility is supported by DST-SERB grant IR/SO/LU-003/2010. The funders had no role in study design, data collection and interpretation, or the decision to submit the work for publication.

Author Contributions: R.V. G.C. and J.B. designed the experiments. G.C. performed the experiments and analyzed the data for Parent inactive mutants, single and double mutants of S12G, single mutants Y8D, V46L, S60E of CcdB and TEM-1 β-lactamase mutants and mRBD mutants. J.B. performed the experiments and analyzed the data for, single and double mutants of E11R. G.C. and J.B. purified the p53-DBD mutants and J.B. performed the experiments and analyzed the data for the p53-DBD mutants. G.C. and J.B. purified the S12G, V46L and S60E for crystal set up and K.M. and P.G. screened the conditions, set up the crystals and solved the structure for S12G, V46L and S60E. K.M. did the Rosetta calculations for all the mutants and the MD simulations. S.A. cloned and purified the Y8D, V46L, S60E CcdB mutants and the mRBD mutants. R.V, G.C., J.B. wrote most of the manuscript with critical inputs and review from all other authors.

Acknowledgements G.C. and J.B. acknowledge Ministry of Human Resource Development for their fellowships. S.A. is thankful to Department of Biotechnology (BT/IN/EU-INF/15/RV/19-20) for his research fellowship. K.M. is thankful to Department of Science and Technology (DST)–Science and Engineering Research Board for financial support, sanction order no: PDF/2017/002641. Dr. Parveen Goyal is supported by the DBT/Wellcome Trust India Alliance Fellowship [grant number IA/E/16/1/502999]. We are thankful to Dr. Sivaramaiah Nallapeta, Head Business Operations, Nano Temper Technologies and Dr. Saji Menon, Application Specialist, Nano Temper Technologies for the nano-DSF and MST facility. Prof. S. Ramaswamy, Senior Professor, Institute of Stem cell Science and Regenerative Medicine is acknowledged for the use the X-ray crystallography facility for the diffraction data collection for the S12G mutant. For the V46L mutant, data was collected at the Elettra synchrotron facility, for S60E data was collected at home source, MBU, IISc. We acknowledge them all. We thank the beamline staff at the Elettra XRD2 particularly Dr. Raghurama Hegde for beamline support. Access to the XRD2 beamline at the Elettra synchrotron, Trieste was made possible through a grant-in-aid from the Department of Science and Technology, India, vide grant number DSTO-1668. We thank Dr. Mahavir Singh, (Indian Institute of Science) for providing the BL21-Rosetta (DE3) strain. Transfection of the mRBD was carried out by Mohammad Suhail Khan and Kawkab Kanjo assisted with ProteOn Studies. We thank them both. The assistance of Nonavinakere Seetharam Srilatha is duly acknowledged for the SPR experiments. We thank Arunabh Athreya for helping with the data collection for V46L mutant at the synchrotron facility. We also thank all the members of the RV lab for their valuable suggestions.

Statistical analysis

All the experiments are carried out in biological replicates (n=2), and the listed errors are the standard error derived from the values obtained for individual replicates. For the nanoDSF and MST measurements, each experiment has been carried out twice, each time with two sets of capillaries (n=4) and the listed errors are the standard error derived from the values obtained for individual replicates. The SPR experiments in Figure S4 have been performed once at each concentration with four different concentrations of the protein and the listed error is the standard error derived from the values at multiple concentrations. The P values for comparing the kinetic parameters, were analysed with a two-tailed Mann Whitney test using the GraphPad Prism software 8.0.0 (* indicates $P < 0.05$, ** indicates $P < 0.005$, *** indicates $P < 0.0005$).

References:

1. Melero C, Ollikainen N, Harwood I, Karpiak J, Kortemme T. Quantification of the transferability of a designed protein specificity switch reveals extensive epistasis in molecular recognition. Proc Natl Acad Sci. 2014;111(43):15426–31.
2. Sahoo A, Khare S, Devanarayanan S, Jain PC. Residue proximity information and protein model discrimination using saturation-suppressor mutagenesis. Elife. 2015;4:e09532.
3. Melamed D, Young DL, Miller CR, Fields S. Combining Natural Sequence Variation with High Throughput Mutational Data to Reveal Protein Interaction Sites. PLoS Genet. 2015;11(2):1–21.
4. Poon A, Davis BH, Chao L. The coupon collector and the suppressor mutation: Estimating the number of compensatory mutations by maximum likelihood. Genetics. 2005;170(3):1323–32.
5. Araya CL, Fowler DM, Chen W, Muniez I, Kelly JW, Fields S. A fundamental protein property, thermodynamic stability, revealed solely from large-scale measurements of protein function. Proc Natl Acad Sci. 2012;109(42):16858–63.
6. Hecht MH, Sauer RT. Phage lambda repressor revertants. Amino acid substitutions that restore activity to mutant proteins. J Mol Biol. 1985;186(1):53–63.
7. Sideraki V, Huang W, Palzkill T, Gilbert HF. A secondary drug resistance mutation of TEM-1 β-lactamase that suppresses misfolding and aggregation. Proc Natl Acad Sci. 2001;98(1):283–8.
8. Bershtein S, Goldin K, Tawfik DS. Intense Neutral Drifts Yield Robust and Evolvable Consensus Proteins. J Mol Biol. 2008;379(5):1029–44.
9. Tripathi A, Gupta K, Khare S, Jain PC, Patel S, Kumar P, et al. Molecular Determinants of Mutant Phenotypes, Inferred from Saturation Mutagenesis Data. Mol Biol Evol. 2016;33(11):2960–75.
10. Bernard P CM. Cell killing by the F plasmid CcdB protein involves poisoning of DNA-topoisomerase II complexes. J Mol Biol. 1992;226(3):735–745.
11. Bajaj K, Chakshusmathi G, Bachhawat-Sikder K, Surolia A, Varadarajan R. Thermodynamic Characterization of Monomeric and Dimeric Forms of CcdB. Biochem J. 2004;380(Pt 2):409–17.
12. Jain PC, Varadarajan R. A rapid, efficient, and economical inverse polymerase chain reaction-based method for generating a site saturation mutant library. Anal Biochem. 2014;449(1):90–8.
13. Adkar B V., Tripathi A, Sahoo A, Bajaj K, Goswami D, Chakrabarti P, et al. Protein model

discrimination using mutational sensitivity derived from deep sequencing. Structure. 2012;20(2):371–81.

14. Ahmed S, Manjunath K, Varadarajan R. Stabilizing proteins through saturation suppressor mutagenesis. bioRxiv. 2021 Jan 1;2021.08.07.455542.
15. Niesen FH, Berglund H VM. The use of differential scanning fluorimetry to detect ligand interactions that promote protein stability. Nat Protoc. 2007;9(2):2212–21.
16. Baliga C, Varadarajan R, Aghera N. Homodimeric Escherichia coli Toxin CcdB (Controller of Cell Division or Death B Protein) Folds via Parallel Pathways. Biochemistry. 2016;55(43):6019–31.
17. Chattopadhyay G, Varadarajan R. Facile measurement of protein stability and folding kinetics using a nano differential scanning fluorimeter. Protein Sci. 2019;28(6):1127–34.
18. Huang W, Petrosino J, Hirsch M, Shenkin PS, Palzkill T. Amino acid sequence determinants of β-lactamase structure and activity. J Mol Biol. 1996;258(4):688–703.
19. Vanhove M, Raquet X, Frère J -M. Investigation of the folding pathway of the TEM-1 β-lactamase. Proteins Struct Funct Bioinforma. 1995;22(2):110–8.
20. Vanhove M, Lejeune A, Pain RH. Beta-Lactamases As Models for Protein-Folding Studies. Cell Mol Life Sci. 1998;54(4):372–7.
21. Wang X, Minasov G, Shoichet BK. Evolution of an antibiotic resistance enzyme constrained by stability and activity trade-offs. J Mol Biol. 2002;320(1):85–95.
22. Marciano DC, Pennington JM, Wang X, Wang J, Chen Y, Thomas VL, et al. Genetic and Structural Characterization of an L201P Global Suppressor Substitution in TEM-1 β -Lactamase. J Mol Biol. 2008;384(1):151–64.
23. Knies JL, Cai F, Weinreich DM. Enzyme Efficiency but Not Thermostability Drives Cefotaxime Resistance Evolution in TEM-1 β-Lactamase. Mol Biol Evol. 2017;34(5):1040–54.
24. Huang W, Palzkill T. A natural polymorphism in β-lactamase is a global suppressor. Proc Natl Acad Sci U S A. 1997;94(16):8801–6.
25. Brown NG, Pennington JM, Huang W, Ayvaz T, Palzkill T. Multiple Global Suppressors of Protein Stability Defects Facilitate the Evolution of Extended-Spectrum TEM β-Lactamases. J Mol Biol. 2010;404(5):832–46.
26. Wang X, Minasov G, Shoichet BK. The structural bases of antibiotic resistance in the clinically derived mutant β-lactamases TEM-30, TEM-32, and TEM-34. J Biol Chem. 2002;277(35):32149–56.
27. Baroni TE, Wang T, Qian H, Dearth LR, Truong LN, Zeng J, et al. A global suppressor motif

for p53 cancer mutants. Proc Natl Acad Sci. 2004;101(14):4930–5.
28. Nikolova P, Henckel J, Lane D, Fersht A. Semirational design of active tumor suppressor p53 DNA binding. Proc Natl Acad Sci. 1998;95:14675–80.
29. Pérez Cañadillas JM, Tidow H, Freund SMV, Rutherford TJ, Ang HC, Fersht AR. Solution structure of p53 core domain: Structural basis for its instability. Proc Natl Acad Sci. 2006;103(7):2109–14.
30. Nikolova P V, Wong K, Dedecker B, Henckel J, Fersht AR. Mechanism of rescue of common p53 cancer mutations by second-site suppressor mutations. EMBO J. 2000;19(3):370–8.
31. Brachmann RK, Yu K, Eby Y, Pavletich NP, Boeke JD. Genetic selection of intragenic suppressor mutations that reverse the effect of common p53 cancer mutations. EMBO J. 1998;17(7):1847–59.
32. Wallentine BD, Wang Y, Tretyachenko-Ladokhina V, Tan M, Senear DF, Luecke H. Structures of oncogenic, suppressor and rescued p53 core-domain variants: Mechanisms of mutant p53 rescue. Acta Crystallogr Sect D Biol Crystallogr. 2013;69(10):2146–56.
33. Malladi SK, Singh R, Pandey S, Gayathri S, Kanjo K, Ahmed S, et al. Design of a highly thermotolerant, immunogenic SARS-CoV-2 spike fragment. J Biol Chem. 2021;296(2021): 10025.
34. Shindyalov IN, Kolchanov NA, Sander C. Can three-dimensional contacts in proteins structures be predicted by analysis of correlated mutations? Protein Eng. 1994;7(3):349–58.
35. Bank C, Hietpas RT, Jensen JD, Bolon DNA. A Systematic Survey of an Intragenic Epistatic Landscape. Mol Biol Evol. 2015;32(1):229–38.
36. Shortle D. Guanidine hydrochloride denaturation studies of mutant forms of staphylococcal nuclease. J Cell Biochem. 1986;30(4):281–9.
37. Pakula AA, Sauer RT. Amino Acid Substitutions That Increase the Thermal Stability of the lambda Cro Protein. Proteins Struct Funct Bioinforma. 1989;5(3):202–210.
38. Brown NG, Pennington JM, Huang W, Ayvaz T, Palzkill T. Multiple Global Suppressors of Protein Stability Defects Facilitate the Evolution of Extended-Spectrum TEM β-Lactamases. J Mol Biol. 2010;404(5):832–46.
39. Tokuriki N, Tawfik DS. Protein dynamism and evolvability. Science. 2009;324(5924): 203–7.
40. Bajaj K, Dewan PC, Chakrabarti P, Goswami D, Barua B, Baliga C, et al. Structural correlates of the temperature sensitive phenotype derived from saturation mutagenesis studies of CcdB. Biochemistry. 2008;47(49):12964–73.
41. Bershtein S, Segal M, Bekerman R, Tokuriki N, Tawfik DS. Robustness-epistasis link shapes the fitness landscape of a randomly drifting protein. Nature. 2006;444(7121):929–32.

42. Sanchez-Ruiz JM. Protein kinetic stability. Biophysical Chemistry. 2010;148(1-3):1–15.
43. Jaswal SS, Sohl JL, Davis JH, Agard DA. Energetic landscape of α-lytic protease optimizes longevity through kinetic stability. Nature. 2002;415(6869):343–6.
44. Lee C, Park S-H, Lee M-Y, Yu M-H. Regulation of protein function by native metastability. Proc Natl Acad Sci. 2000;97(14):7727–31.
45. Chan DC, Fass D, Berger JM, Kim PS. Core structure of gp41 from the HIV envelope glycoprotein. Cell. 1997;89(2):263–73.
46. Bullough PA, Hughson FM, Skehel JJ WD. Structure of influenza haemagglutinin at the pH of membrane fusion. Nature. 1994;371(6492):37–43.
47. Leikina E, Mertts M V., Kuznetsova N, Leikin S. Type I collagen is thermally unstable at body temperature. Proc Natl Acad Sci. 2002;99(3):1314–8.
48. Persikov A V., Brodsky B. Unstable molecules form stable tissues. Proc Natl Acad Sci. 2002;99(3):1101–3.
49. Lynch SM, Boswell SA, Colón W. Kinetic stability of Cu/Zn superoxide dismutase is dependent on its metal ligands: Implications for ALS. Biochemistry. 2004;43(51):16525–31.
50. Lynch SM, Colón W. Dominant role of copper in the kinetic stability of Cu/Zn superoxide dismutase. Biochem Biophys Res Commun. 2006;340(2):457–61.
51. Ionescu RM, Vlasak J, Price C KM. Contribution of variable domains to the stability of humanized IgG1 monoclonal antibodies. J Pharm Sci. 2008;97(4):1414–26.
52. Contessoto VG, de Oliveira VM, Fernandes BR, Slade GG, Leite VBP. TKSA-MC: A web server for rational mutation through the optimization of protein charge interactions. Proteins Struct Funct Bioinforma. 2018;86(11):1184–8.
53. Pettersen E., Goddard T., Huang C., Couch G., Greenblatt D., Meng E., et al. UCSF Chimera — A visualization system for exploratory research and analysis. J Comput Chem. 2004;25(13):1605–12.
54. Fedorov AN, Baldwin TO. Cotranslational protein folding. Journal of Biological Chemistry. 1997;272(52):32715–8.
55. Ahmed S, Manjunath K, Varadarajan R. Prediction of residue-specific contributions to binding and thermal stability using yeast surface display. bioRxiv. 2021 Jan 1;2021.05.31.446445.
56. Boysen M, Kityk R, Mayer MP. Hsp70- and Hsp90-Mediated Regulation of the Conformation of p53 DNA Binding Domain and p53 Cancer Variants. Mol Cell. 2019;74(4):831–843.e4.
57. Butler JS, Loh SN. Kinetic partitioning during folding of the p53 DNA binding domain. J Mol Biol. 2005;350(5):906–18.

58. Walerych D, Olszewski MB, Gutkowska M, Helwak A, Zylicz M, Zylicz A. Hsp70 molecular chaperones are required to support p53 tumor suppressor activity under stress conditions. Oncogene. 2009;28(48):4284–94.
59. Bochkareva ES, Lissin NM, Girshovich AS. Transient association of newly synthesized unfolded proteins with the heat-shock GroEL protein. Nature. 1988;336(6196):254–7.
60. Laminet AA, Ziegelhoffer T, Georgopoulos C, Pluckthun A. The Escherichia coli heat shock proteins GroEL and GroES modulate the folding of the β-lactamase precursor. EMBO J. 1990;9(7):2315–9.
61. Consortium AA. Structural and functional comparison of SARS-CoV-2-spike receptor binding domain produced in Pichia pastoris and mammalian cells. Sci Rep. 2020;10(1):21779.
62. Khlebnikov A, Datsenko KA, Skaug T, Wanner BL, Keasling JD. Homogeneous expression of the PBADpromoter in Escherichia coli by constitutive expression of the low-affinity high-capacity araE transporter. Microbiology. 2001;147(12):3241–7.
63. Bullock AN, Henckel J, Fersht AR. Quantitative analysis of residual folding and DNA binding in mutant p53 core domain: Definition of mutant states for rescue in cancer therapy. Oncogene. 2000;19(10):1245–56.
64. Tripathi A, Swaroop S, Varadarajan R. Molecular Determinants of Temperature-Sensitive Phenotypes. Biochemistry. 2019;58(13):1738–50.
65. Rathore U, Saha P, Kesavardhana S, Kumar AA, Datta R. Glycosylation of the core of the HIV-1 envelope subunit protein gp120 is not required for native trimer formation or viral infectivity. J Biol Chem. 2017;292:10197–219.
66. Lindahl E, Abraham MJ HBV der S. GROMACS 2019.2 Source Code. 2019.
67. Kaminski GA, Friesner RA, Tirado-Rives J, Jorgensen WL. Evaluation and reparametrization of the OPLS-AA force field for proteins via comparison with accurate quantum chemical calculations on peptides. J Phys Chem B. 2001;105(28):6474–87.
68. Jorgensen WL, Chandrasekhar J, Madura JD, Impey RW, Klein ML. Comparison of simple potential functions for simulating liquid water. J Chem Phys. 1983;79(2):926–35.
69. Darden T, York D, Pedersen L. Particle mesh Ewald: An N·log(N) method for Ewald sums in large systems. J Chem Phys. 1993;98(12):10089–92.
70. Nosé S. A unified formulation of the constant temperature molecular dynamics methods. J Chem Phys. 1984;81(1):511–9.
71. Hoover WG. Canonical dynamics: Equilibrium phase-space distributions. Phys Rev A. 1985;31(3):1695–7.
72. Parrinello M, Rahman A. Polymorphic transitions in single crystals: A new molecular

dynamics method. J Appl Phys. 1981;52(12):7182–90.

73. Winn MD, Ballard CC, Cowtan KD, Dodson EJ, Emsley P, Evans PR, et al. Overview of the CCP4 suite and current developments. Acta Crystallogr Sect D Biol Crystallogr. 2011;67(Pt4):235–42.
74. Battye TGG, Kontogiannis L, Johnson O, Powell HR, Leslie AGW. iMOSFLM: A new graphical interface for diffraction-image processing with MOSFLM. Acta Crystallogr Sect D Biol Crystallogr. 2011;67(4):271–81.
75. McCoy AJ, Grosse-Kunstleve RW, Adams PD, Winn MD, Storoni LC, Read RJ. Phaser crystallographic software. J Appl Crystallogr. 2007;40(4):658–74.
76. Loris R, Dao-Thi M-H, Bahassi EM, Van Melderen L, Poortmans F, Liddington R, et al. Crystal structure of CcdB, a topoisomerase poison from E.coli. J Mol Biol. 1999;285(4):1667–77.
77. Murshudov GN, Vagin AA, Dodson EJ. Refinement of macromolecular structures by the maximum-likelihood method. Vol. 53, Acta Crystallographica Section D: Biological Crystallography. 1997. p. 240–55.
78. Murshudov GN, Skubák P, Lebedev AA, Pannu NS, Steiner RA, Nicholls RA, et al. REFMAC5 for the refinement of macromolecular crystal structures. Acta Crystallogr Sect D Biol Crystallogr. 2011;67(4):355–67.
79. Emsley P, Cowtan K. Coot: Model-building tools for molecular graphics. Acta Crystallogr Sect D Biol Crystallogr. 2004;60(12 I):2126–32.
80. Emsley P, Lohkamp B, Scott WG, Cowtan K. Features and development of Coot. Acta Crystallogr Sect D Biol Crystallogr. 2010;66(4):486–501.
81. Fonze E, Charlier P, To'th Y, Vermeire M, Raquet X, Dubus A, et al. TEM1 beta-lactamase structure solved by molecular replacement and refined structure of the S235A mutant. Acta Crystallogr Sect D Biol Crystallogr. 1995;51(5):682–94.
82. Wang Y, Rosengarth A, Luecke H. Structure of the human p53 core domain in the absence of DNA. Acta Crystallogr Sect D Biol Crystallogr. 2007;63(3):276–81.
83. Zhou D, Duyvesteyn HME, Chen CP, Huang CG, Chen TH, Shih SR, et al. Structural basis for the neutralization of SARS-CoV-2 by an antibody from a convalescent patient. Nat Struct Mol Biol. 2020;27(10):950–8.
84. Wienken CJ, Baaske P, Rothbauer U, Braun D, Duhr S. Protein-binding assays in biological liquids using microscale thermophoresis. Nat Commun. 2010;1(7):1–7.

Figures

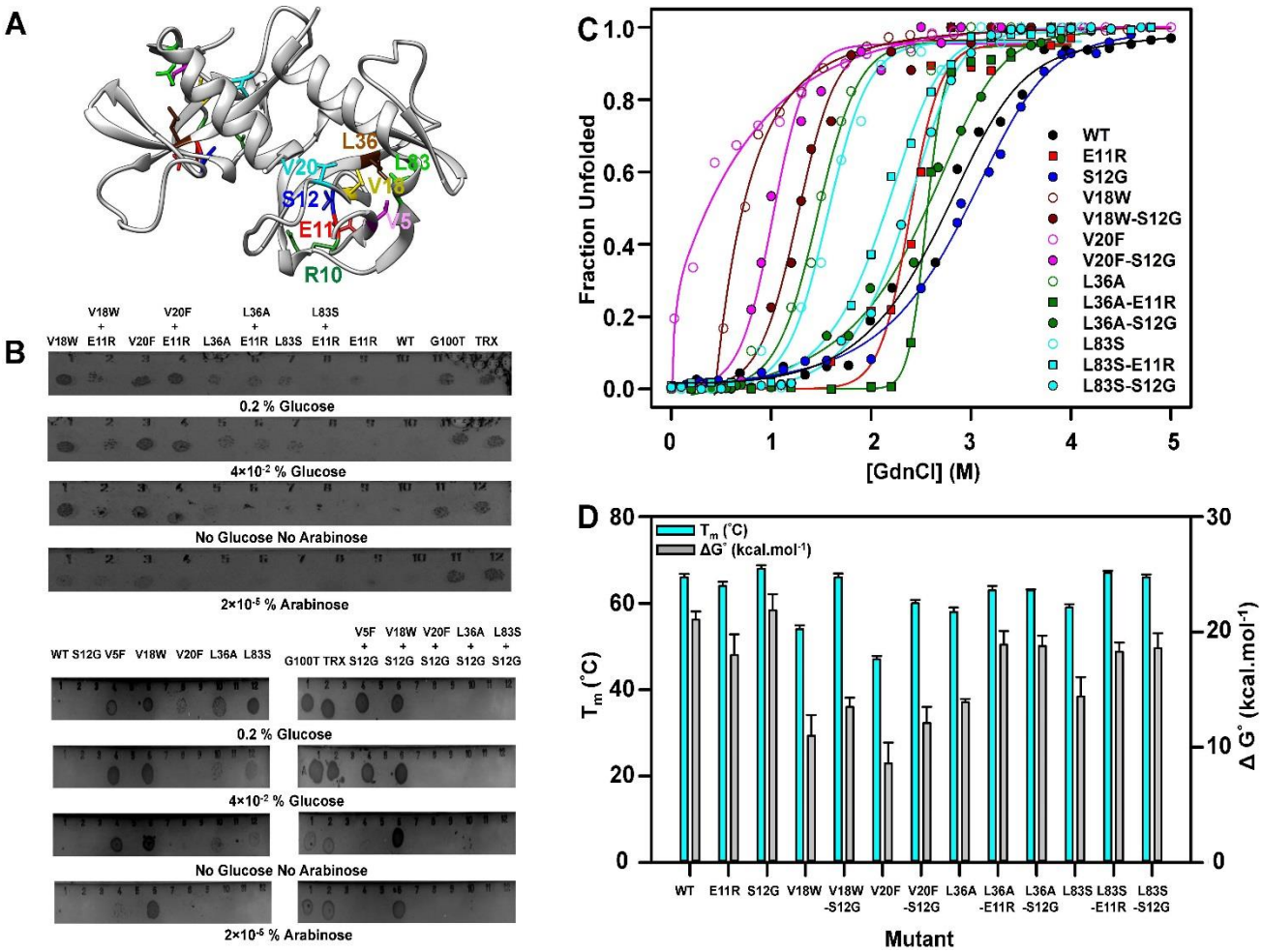

Figure 1. **Folding defects rescued by suppressors.** (A) Experimentally obtained inactive mutants and distal suppressors mapped onto the crystal structure of CcdB (PDB ID 3VUB [Loris et al., 1999]). The CcdB protein is shown in ribbon with the distal suppressors R10, E11and S12 mapped on an exposed loop region while the PIMs V5, V18 V20, L36A and L83S are present in the core of the protein. The residues highlighted are shown in the context of the CcdB homodimer. (B) *In-vivo* activity of the PIMs at 37 °C in the background of the suppressor E11R and S12G. The condition where growth ceased was reported as the active condition. Four representative conditions are shown. Cells transformed with G100T, inactive mutant and *E.coli* thioredoxin (TRX) expressing plasmids are shown as non-toxic controls which grow under all conditions. (C) Equilibrium GdnCl denaturation profiles carried out in 200 mM HEPES pH 8.4, at 25 ˚C using 5 µM of purified proteins using nanoDSF is shown. The

experimental data are shown in symbols, while the fits are shown in solid lines. (D) Thermal stability, T_m (in cyan) and thermodynamic stability, ΔG° (in grey) of the different CcdB mutants . The error bars wherever shown represent the standard deviation from two independent experiments, each performed in duplicates. *See also Figure S1*.

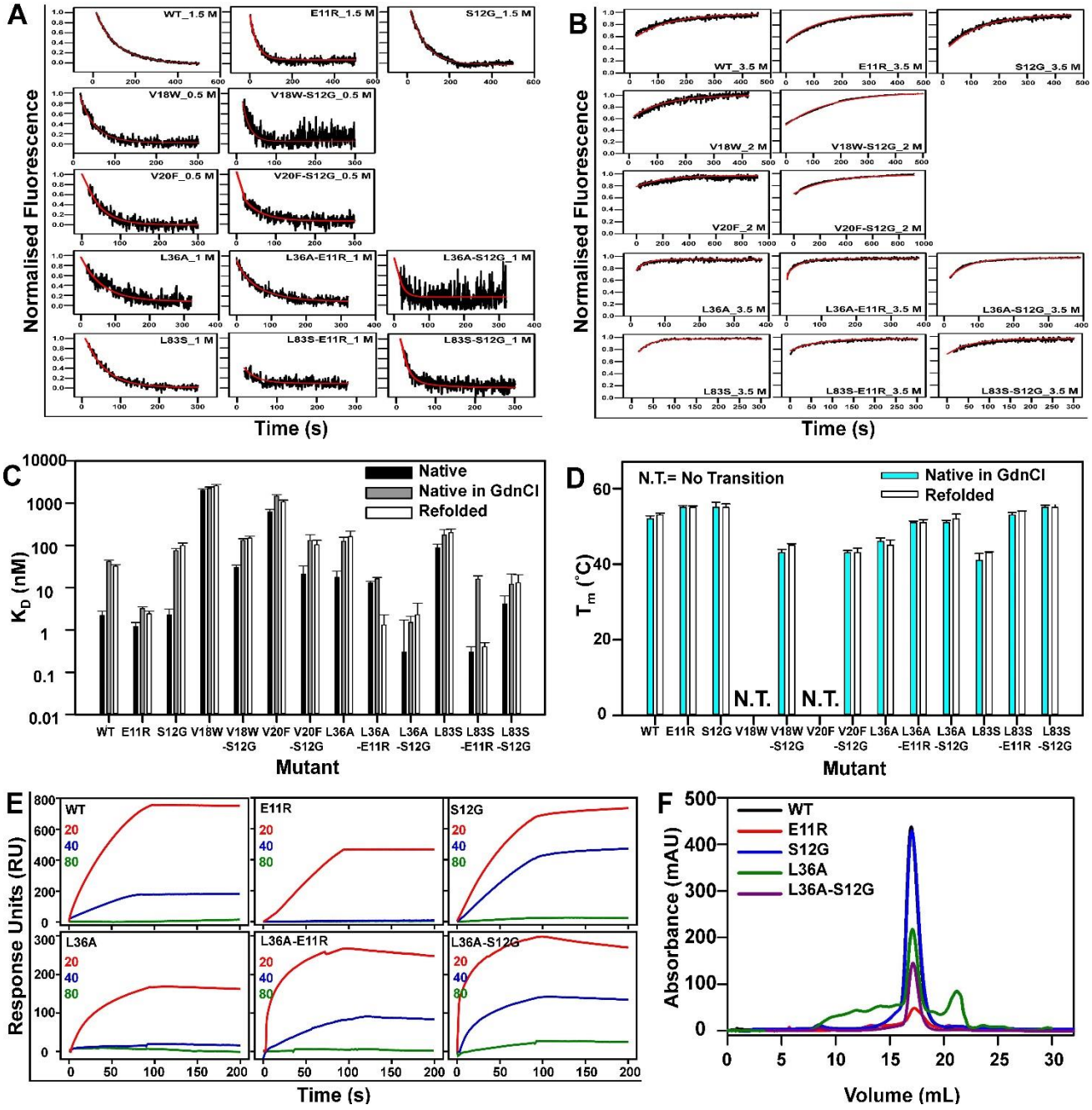

Figure 2: Kinetic and thermodynamic stabilisation by the CcdB suppressor mutants. (A) CcdB proteins exhibit biphasic refolding kinetics with a fast and slow phase whereas (B) unfolding of CcdB proteins follows single exponential kinetics. Representative kinetic traces at 5 μM protein concentration of WT and selected CcdB mutants are shown. The experimental kinetic traces obtained at different GdnCl concentrations are shown in black, while the fits are shown in red**.** The measured kinetic parameters are listed in Table 2. (C) Interaction between native (black), native protein in GdnCl (grey) and refolded (white) CcdB mutant proteins and labeled Gyrase A-14 (70 nM) analyzed by MST.

(D) The apparent thermal melting temperatures (T_m) for native proteins in GdnCl (cyan) and refolded proteins (grey). The error bars represent the standard deviation from two independent experiments, each performed in duplicates. (E) Binding of 500 nM WT and mutant CcdB to immobilised GyraseA-14.measured by passing the same concentrations of the analyte (CcdB proteins), after heat stress at two different temperature (40 and 80 °C), followed by cooling back to 25 °C. A room temperature control (25 °C) was also used. The residual active fraction was calculated as described in the materials section. (see Table S5). (F) The SEC profiles of a few of the CcdB mutants are shown. The PIM L36A shows aggregation as well as degradation as compared to the WT and E11R, S12G suppressors. The L36A-S12Ghas a similar profile like the WT and S12G . *See also FigureS1-S4.*

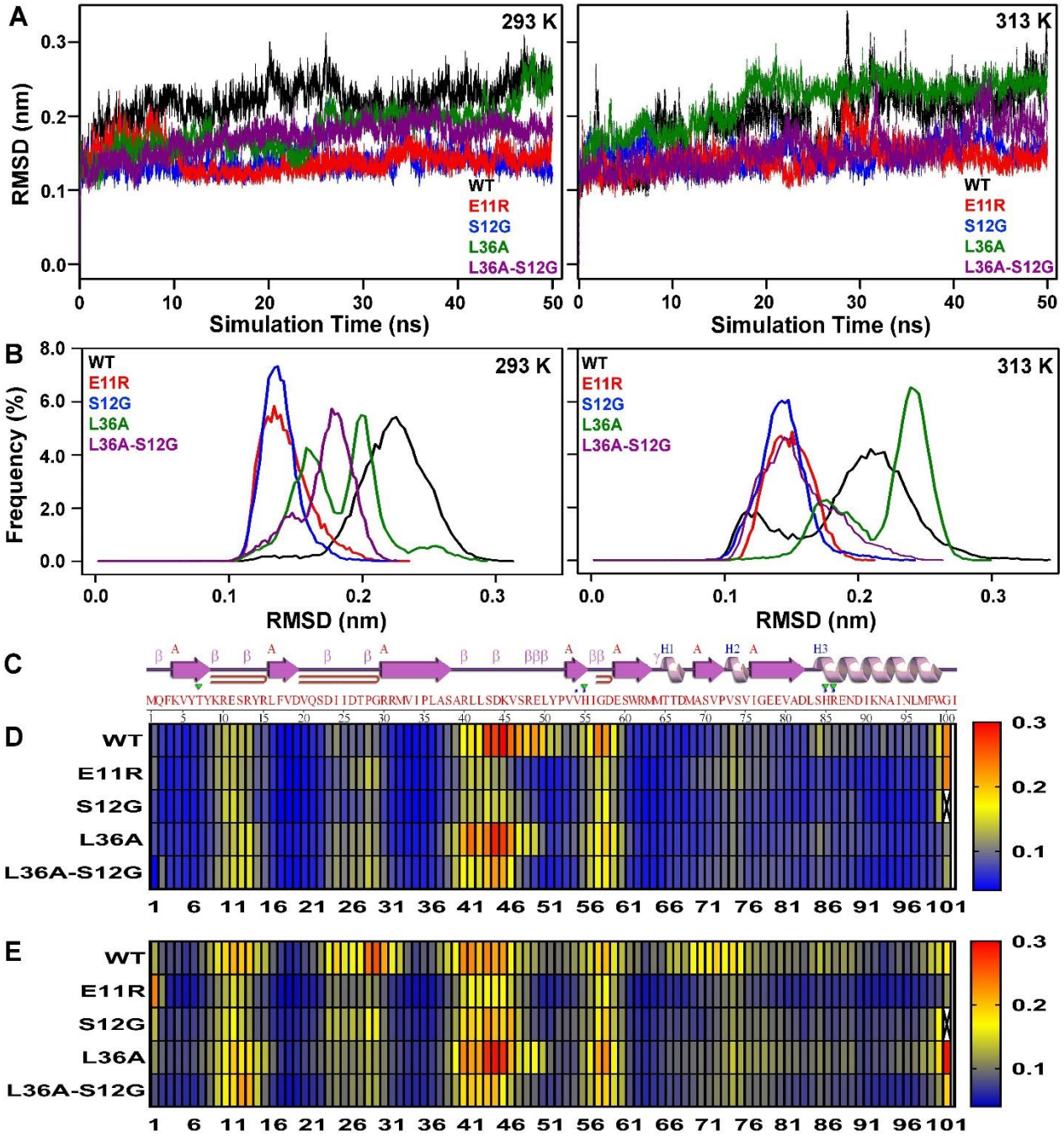

Figure 3. MD simulation analysis of CcdB mutants. (A) Comparison of RMSD values of WT and CcdB mutants calculated from 50-ns MD simulations at 293 K and 313 K. (B) RMSD distribution from 50-ns simulations at 293 K and 313 K. The bin for the distribution is 0.0035 nm. (C) One-dimensional view of the secondary structure of CcdB aligned to its amino acid sequence is shown below. (D-E) Heatmap representing the RMSF of WT and CcdB mutants at 293 K and 313 K respectively. The heatmaps are coloured according to the RMSF value of the residues. Blue to red colour gradation represents increasing RMSF values.

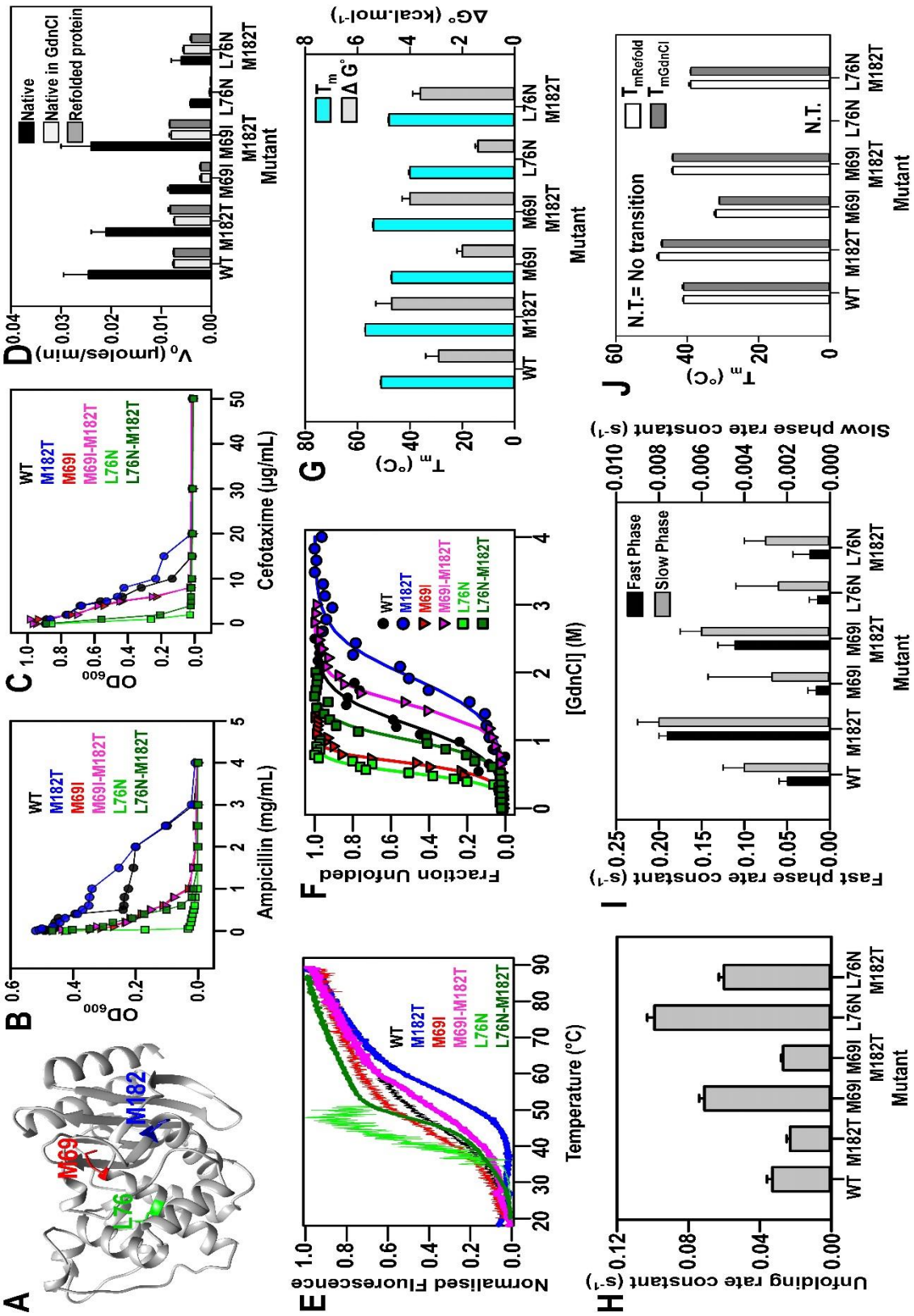

Figure 4. Enhancement of protein stability by M182T global suppressor in extended spectrum TEM-1 β lactamases. (A) Inactive mutants and distal suppressor M182T mapped onto the crystal structure of TEM-1 (PDB ID 1XPB (81)). The TEM-1 protein is shown in ribbon with the distal

suppressor M182T, mapped on an exposed region, while the inactive mutants L76N and M69I are present in the core of the protein. (B-C) Influence of M182T substitution on TEM-1 mediated MIC levels using ampicillin (B) and cefotaxime (C) broth dilutions and pET24a plasmid. (D) The initial velocity (V_0) of the native enzyme (black), protein in 0.5 M GdnCl (light grey) and refolded protein in 0.5 M GdnCl (dark grey) at 25 °C with 10 nM protein and 50 µM of nitrocefin. (E-F) Thermal unfolding profile and equilibrium GdnCl denaturation of 10 µM of purified WT, and TEM-1 β lactamase mutants. (G) Thermal stability, T_m of native proteins (in cyan) and thermodynamic stability, ΔG° (in grey) of the different TEM-1 mutants are plotted. (H-I) The observed rate constants of unfolding (2.5 M GdnCl) and the observed rate constants of the fast phase (black) and slow phase (grey) of refolding (0.5 M GdnCl) of different mutants is represented (Table S6). (J) Thermal stability of 10 µM of native proteins (white) and refolded proteins in 0.5 M GdnCl (grey) are shown. The error bars wherever shown represent the standard deviation from two independent experiments, each performed in duplicates. *See also Figure S5.*

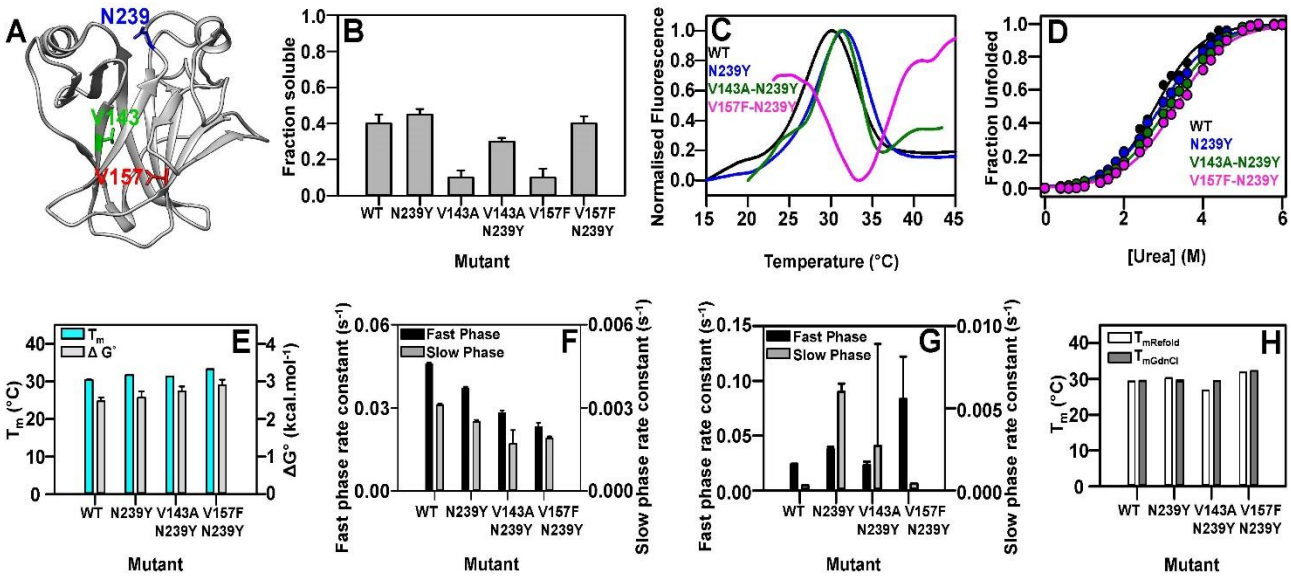

Figure 5. Characterisation of an N239Y global suppressor in DNA Binding Domain of p53. (A) Inactive mutants and distal suppressor N239Y mapped onto the crystal structure of p53-DBD (PDB ID 2OCJ (82)). The p53-DBD is shown in ribbon with the suppressor N239Y, mapped on an exposed region, while the inactive mutants V143A and V157F are present in the core of the protein. (B) Influence of N239Y substitution on p53-DBD solubility levels. (C-D) Thermal unfolding profile and equilibrium Urea denaturation respectively of 10 μM of purified WT and p53-DBD mutants. (E) Thermal stability, T_m of native proteins (in cyan) and thermodynamic stability, ΔG° (in grey) of the different p53-DBD mutants are plotted. (F-G) The observed rate constants of the fast phase (black) and slow phase (grey) of unfolding in 4.4 M Urea (F) and of refolding in 2 M Urea (G) of different mutants is represented (Table S7). (H) Thermal stability of 10 μM of native proteins (white) and refolded proteins in 0.5 M Urea (grey) are shown. The error bars wherever shown represent the standard deviation from two independent experiments, each performed in duplicates. *See also Figure S5.*

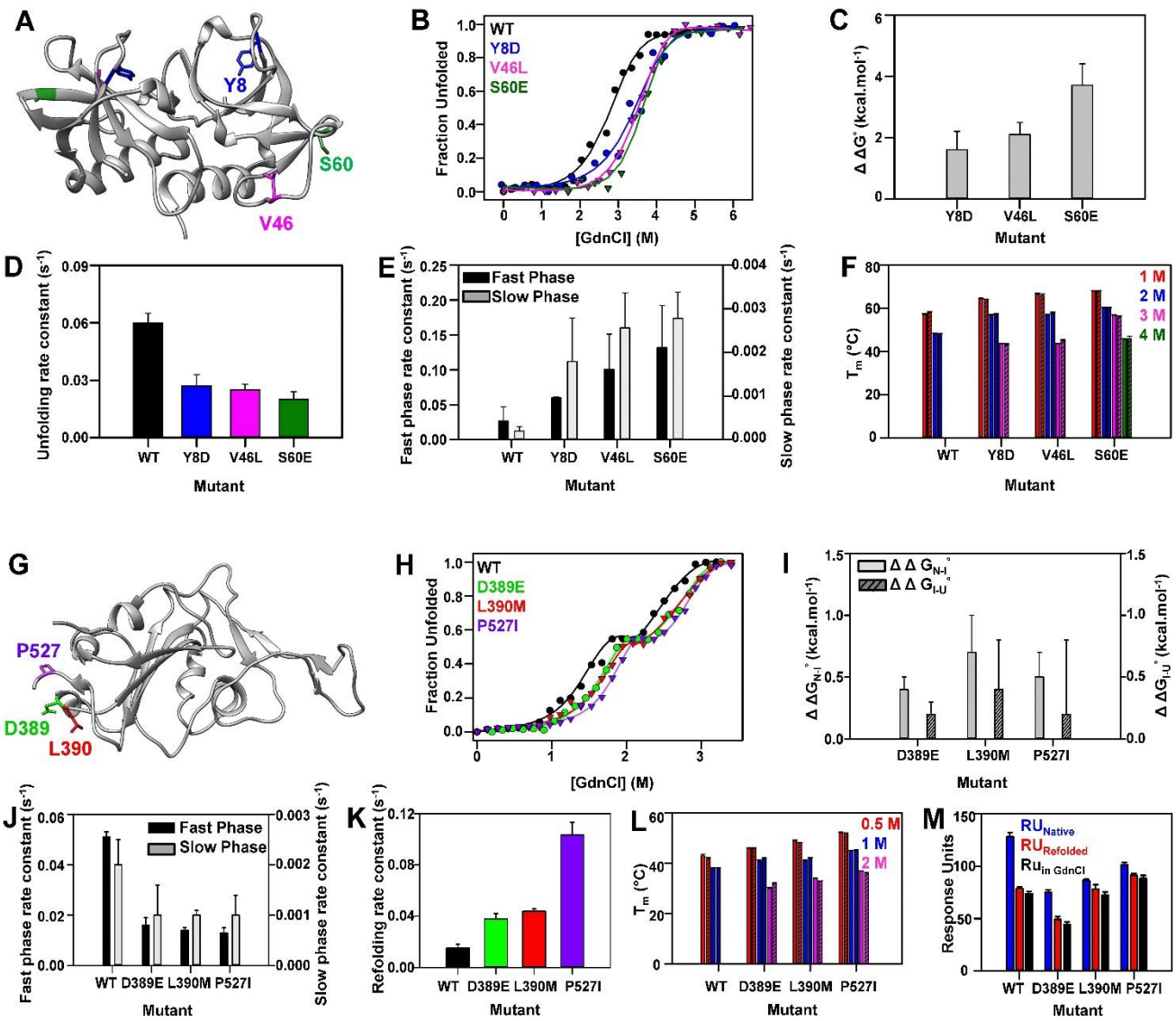

Figure 6. Enhancement in protein stability by highly stable suppressor mutations in CcdB and mRBD.

(A-F) CcdB: (A) The distal suppressors Y8D, V46L, S60E on an exposed region mapped onto the crystal structure of CcdB (PDB ID 3VUB (76)). (B) Equilibrium GdnCl denaturation profiles of 5 µM of CcdB-WT and mutants carried out by nanoDSF. (C) Difference in thermodynamic stability, $\Delta\Delta G^{\circ}$ (in grey) of the different CcdB suppressor mutants are plotted. (D-E) The observed rate constants of unfolding (4.5 M GdnCl) and the observed rate constants of the fast phase (black) and slow phase (grey) of refolding (2 M GdnCl) of different mutants (see also Table S9). (F) Thermal stability, T_m of 5 µM of native proteins in 1 M, 2M, 3M, 4M GdnCl (solid bars) and refolded CcdB proteins in same

concentrations of GdnCl (striped bars). The error bars wherever shown represent the standard deviation from two independent experiments, each performed in duplicates. *See also Figure S6.*

(G-M) mRBD: (G) The distal suppressors D389E, L390M, P527I on an exposed region mapped onto the crystal structure of RBD (PDB ID 6ZER (83)). (H) Equilibrium GdnCl denaturation profile of 5 µM of purified mRBD-WT and mRBD mutants using nanoDSF. The theoretical curves for C_m were obtained by fitting all the melts with three-state unfolding models. (I) Difference in thermodynamic stability, $\Delta\Delta G_{N\text{-}I}^{\circ}$ (grey solid bars) and $\Delta\Delta G_{I\text{-}U}^{\circ}$ (grey striped bars) of the different mRBD suppressor mutants. (J-K) The observed rate constants of fast phase (black) and slow phase (grey) of unfolding (3 M GdnCl) and the observed rate constants of refolding (0.5 M GdnCl) of different mutants (see also Table S9). (L) Thermal unfolding traces of 5 µM of native mRBD proteins in 0.5 M (red), 1M (blue), 2M (pink) GdnCl (solid bars) and refolded mRBD proteins in same concentrations of GdnCl (striped bars). (M) Binding of 50 nM of native mRBD proteins (blue), native mRBD proteins in 0.5 M GdnCl (red solid) and refolded mRBD proteins in 0.5 M GdnCl (red striped) with ACE2-hFc neutralizing antibody is shown. The error bars wherever shown represent the standard deviation from two independent experiments, each performed in duplicates. *See also Figure S6.*

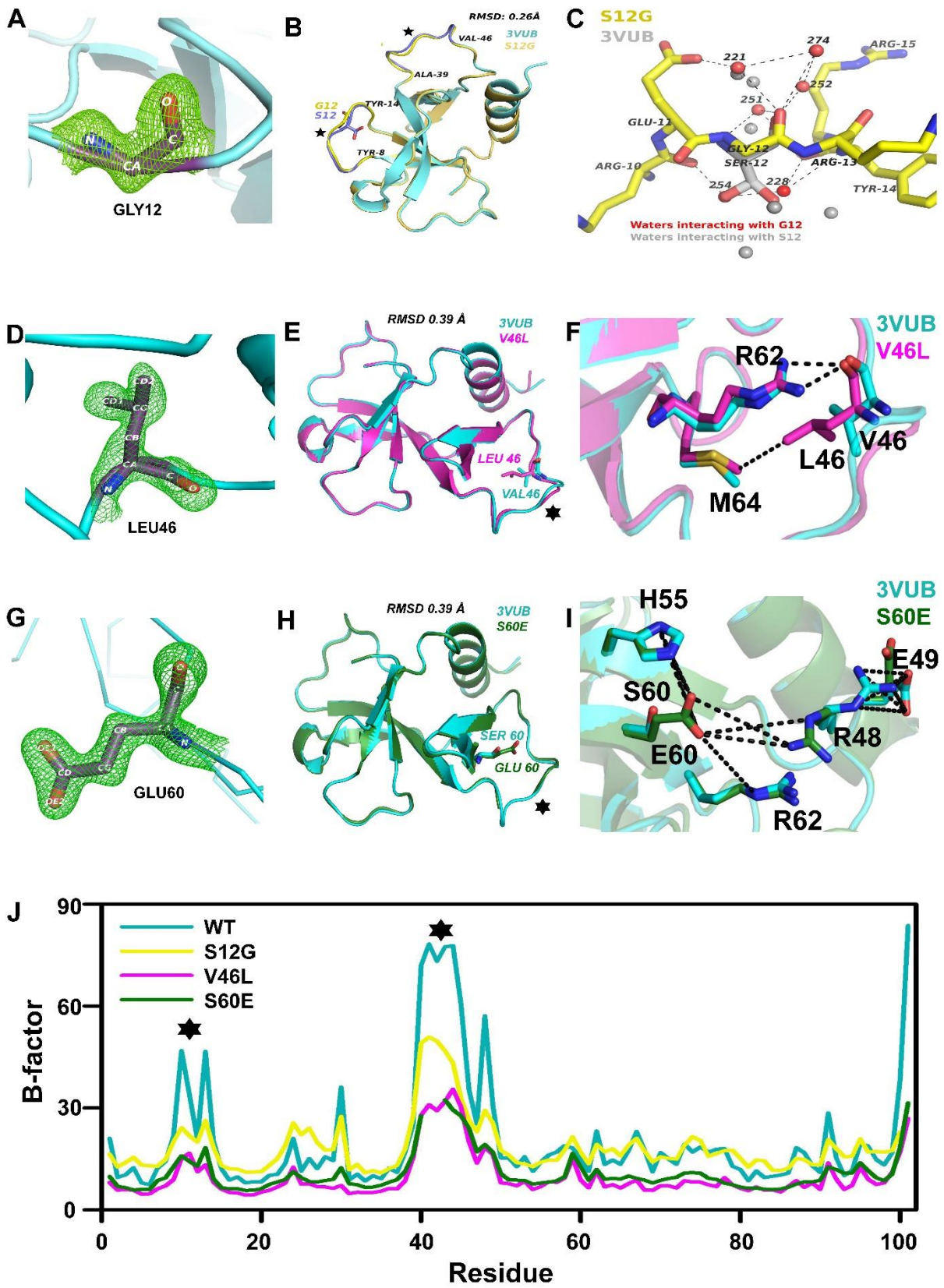

Figure 7. Structures of stabilised CcdB mutants. (A) Composite omit map at residue 12. (B) Structural superposition of WT (3VUB) and S12G monomers, regions displaying deviation are

indicated by ⋆. (C) Network of interactions at the 12th position in S12G. WT structure is shown with a grey backbone. S12 in 3VUB adopts two conformations with partial occupancy, the position of the corresponding hydroxyl group in each conformation is taken up by two water molecules in S12G. Water molecules directly interacting with G12 is shown in red and the corresponding water in 3VUB in grey. (D) Composite omit map at residue 46. (E) Structural superposition of WT and V46L monomers, regions displaying deviation are indicated by ⋆. (F) Network of interactions at the 46th position in V46L. WT structure is shown in cyan. Main chain of L46 is involved in H-bond interactions with side chain nitrogen of R62 and the side chain of L46 is involved in hydrophobic interactions with side chain of M64. (G) Composite omit map at residue 60. (H) Structural superposition of WT and S60E monomers, regions displaying deviation are indicated by ⋆. (I) Network of interactions at the 60th position in S60E. WT structure is shown in cyan. E60 is involved in salt bridge interactions with R48, H55 and R62. (J) Average B-factor plot of the residues in WT, S12G and S60E. Regions with large variability are indicated by "⋆".

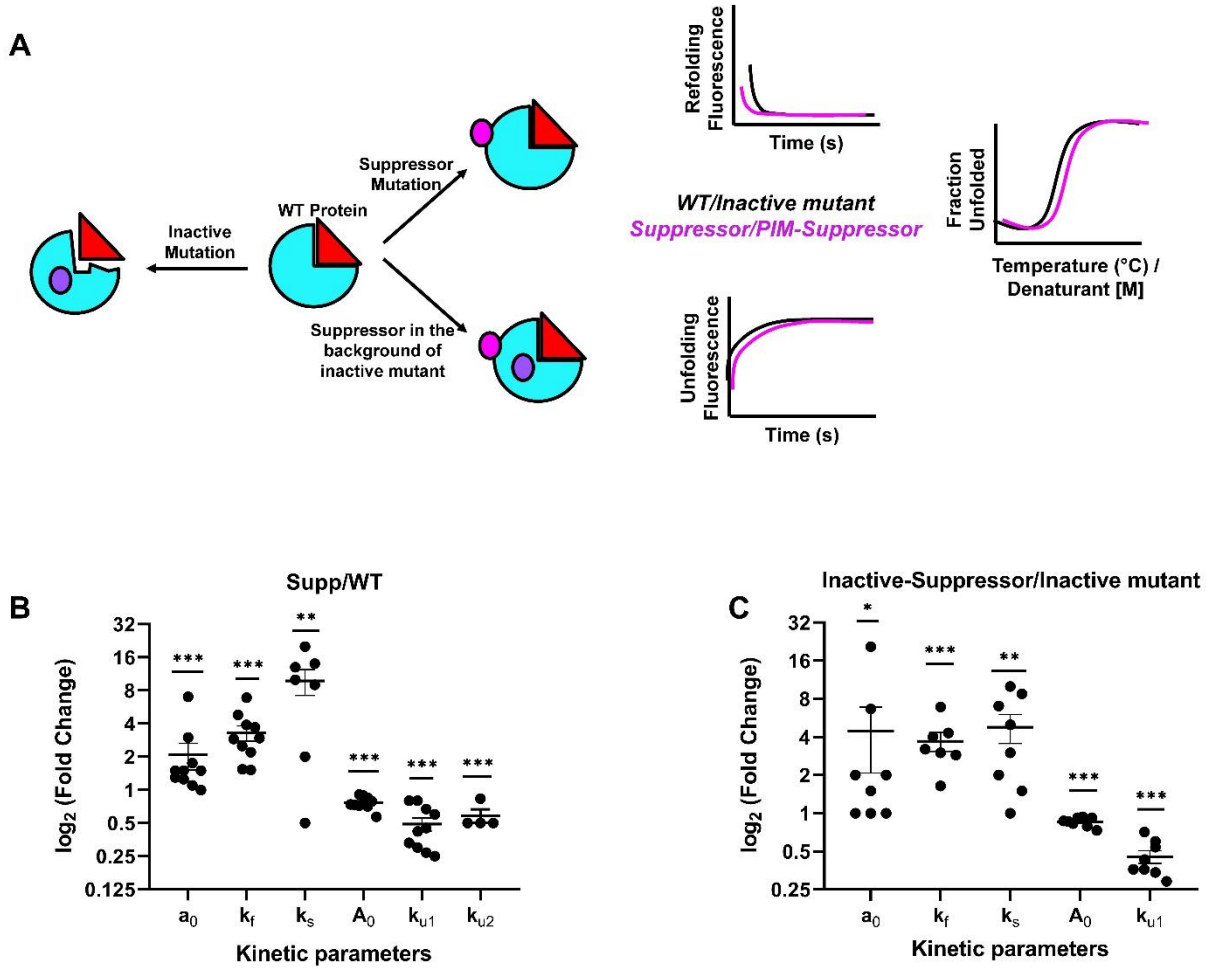

Figure 8. Schematic for mechanism of action of suppressor mutations. (A) The suppressors alone and in the background of the inactive mutants, stabilise the WT protein and the inactive mutants respectively, both thermodynamically and kinetically without losing the activity. The higher kinetic stability is achieved mostly through faster refolding rates. (B-C) Log_2 fold change of various parameters (Mean±SEM) by the suppressor mutations. Mann Whitney non-parametric test was performed for each of these parameters. We observed that the mean of the distributions of the values for each of the parameters are significantly higher than 1 for refolding, and lower than 1 for unfolding. P value indicated with *, ** and *** indicates < 0.05, < 0.005 and < 0.0005 respectively.

Table 1 (Related to Figure 8). Average fold change of various parameters (Mean±SEM) by the suppressor mutations.

Ratio	**Refolding kinetic parameter ratio**			**Unfolding kinetic parameter ratio**		
	Fast		**Slow**	**Fast**		**Slow**
	a_0	k_f	k_s	A_0	k_{u1}	k_{u2}
WT/ Suppressor	2.1±0.6	3.3±0.5	9.8±2.6	0.77±0.03	0.5±0.07	0.6±0.08
PIM/ PIM-Suppressor	4.5±2.4	3.7±0.6	4.8±1.2	0.86±0.03	0.45±0.05	-

Supplementary Figures and Tables

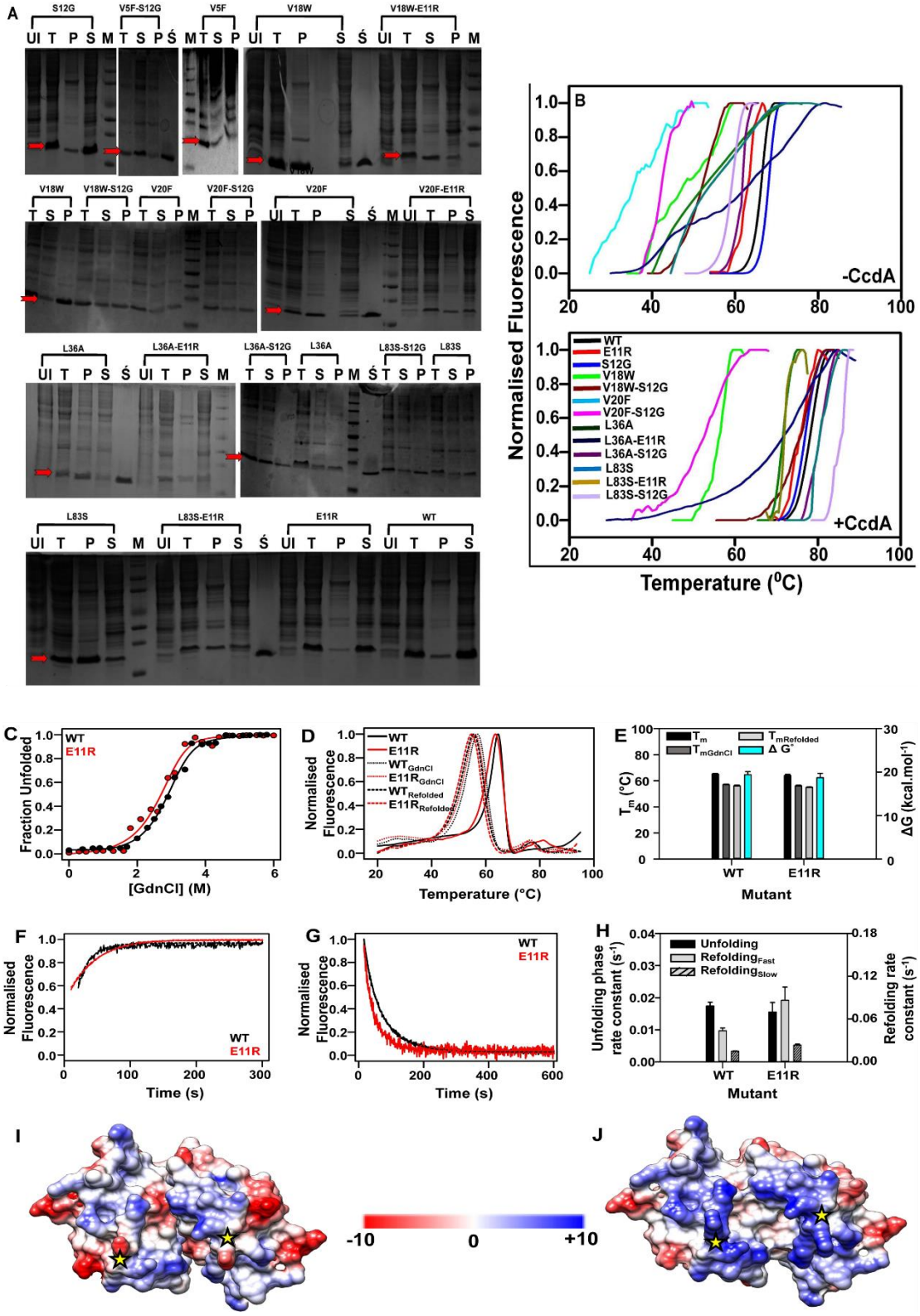

Supplementary Figure S1: Enhancement of solubility and stability by the suppressors (related to Figure 1). (A-B) Solubility and thermal stabilities of CcdB mutants, in presence and absence

of the suppressors (A) *In vivo* solubility estimates for CcdB mutants. UI, T, S and P are uninduced, total cell lysate, supernatant and pellet respectively. Ś is the purified CcdB WT protein used as standard and M is the molecular weight marker lane. The relative estimates of protein present in the soluble fraction and inclusion bodies for all mutants are shown in Table S1. The red arrow indicates the band for the induced protein. (B) Thermal unfolding profile of purified WT CcdB and CcdB mutants in the absence and presence of 8 µM CcdA peptide (45-72) measured by a thermal shift assay (TSA).

(C-J) Effect of E11R suppressor substitution on CcdB stability and folding (C-H): Enhanced stability and folding of suppressor E11R in PBS, pH7.4. (C) Equilibrium GdnCl denaturation profiles using 5 µM of purified WT CcdB and E11R are shown. (D) Thermal unfolding profile of 5 µM of purified WT CcdB and E11R in native form (solid lines), native in GdnCl (dotted lines) and refolded protein (dashed lines) are shown. (E) Thermal stability of native protein, native protein in 1.5 M GdnCl, refolded protein and thermodynamic stability, ΔG° of the WT CcdB and E11R are shown. (F-G) Representative kinetic traces at 5 µM protein concentration of WT CcdB and E11R are shown in presence of 4 M GdnCl for unfolding (F) and 1.5 M GdnCl for refolding (G). (H) The observed rate constants of fast phase and slow phase of refolding in 1.5 M GdnCl and the observed rate constants of unfolding in 4 M GdnCl of WT and E11R (see also Table S4). The error bars wherever shown represent the standard deviation from two independent experiments, each performed in duplicates.

(I-J) Coulombic potential surfaces generated for CcdB WT and E11R using the UCSF Chimera. The coulombic potential surfaces generated were coloured using the colour gradation range from blue (-10 kcal mol^{-1} ε^{-1}) to white (0 kcal mol^{-1} ε^{-1}) to red (+10 kcal mol^{-1} ε^{-1}), where ε is the dielectric constant of the medium (Pettersen et al, 2004). 11th residue is highlighted by yellow star. Potential surface maps of (I) CcdB WT and (J) E11R mutant highlight the appearance of a positive potential patch in the 8-15 loop surrounding the 11th residue in the E11R mutant.

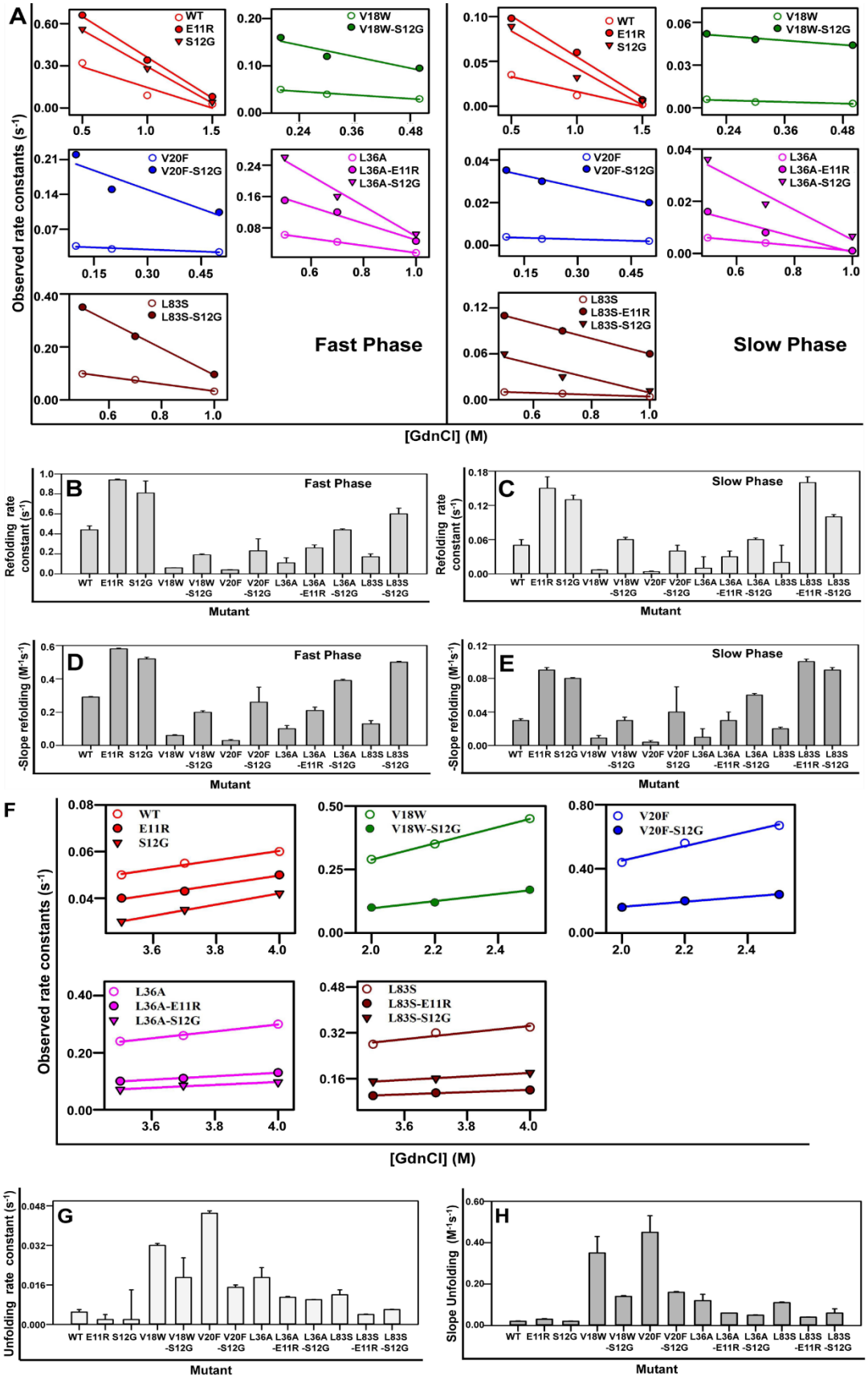

Supplementary Figure S2: Denaturant-dependent refolding and unfolding kinetics of CcdB mutant proteins (related to Figure 2). (A-E) Representative refolding rate constants of fast phase

(left side) and slow phase (right panel) and (F-H) unfolding rate constants at 5 μM protein concentration of the WT and mutants are shown. The experimental rate constants (for refolding and unfolding) obtained at increasing final GdnCl concentrations are shown in dots, while fits are shown in solid lines. For refolding kinetics, the extrapolated rate constants and the magnitude of refolding m-values of the transition states at zero denaturant concentration of fast phase (B and D respectively) and slow phase (C and E respectively) are shown. Suppressor mutations significantly accelerate the refolding rate constants. For unfolding kinetics, the extrapolated rate constants (G) and the magnitude of unfolding m-values (H) at zero denaturant concentration are shown. Suppressor mutations decrease the unfolding rate constants. The error bars wherever shown represent the standard deviation from two independent experiments, each performed in duplicates (see also Table S3).

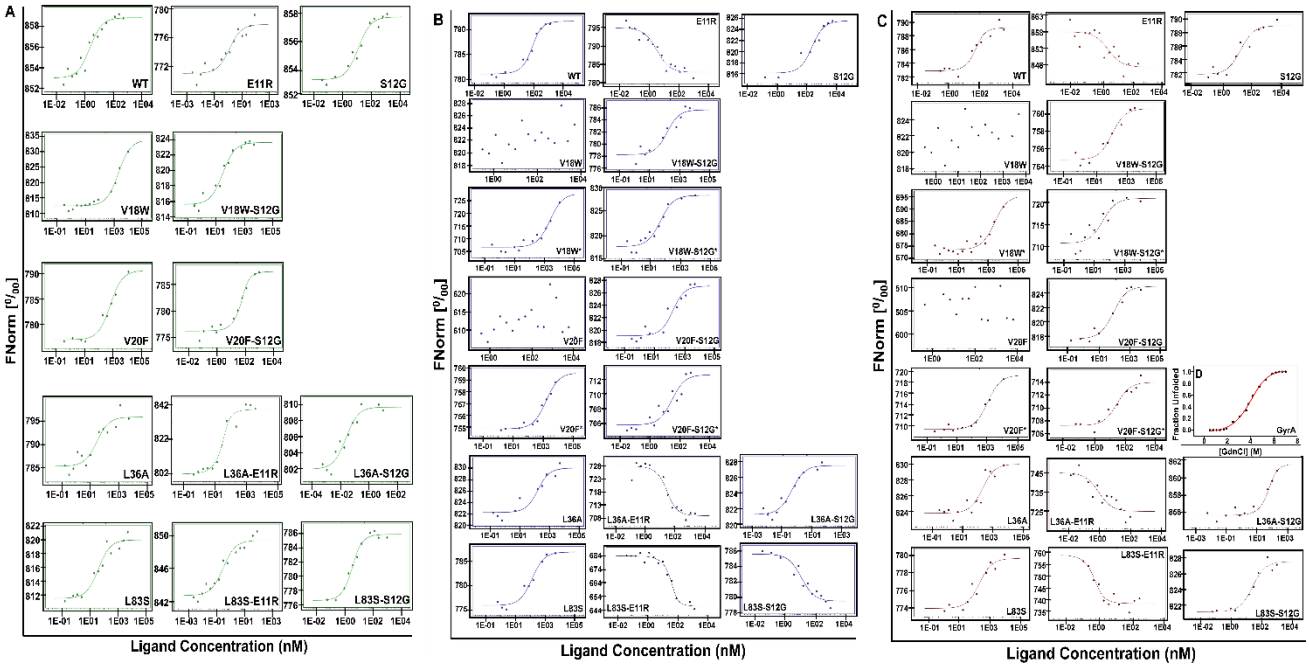

Supplementary Figure S3: Interaction of native, native in the presence of GdnCl and refolded CcdB WT and mutant proteins with labeled Gyrase A-14 analyzed by MicroScale Thermophoresis (related to Figure 2). Gyrase A-14 was labeled and used at a concentration of 70 nM and titrated with different concentrations of native (A), native in the presence of GdnCl (B) and refolded (C) WT and CcdB mutants. All studies were carried out in 200 mM HEPES, pH 8.4, at 27 °C. The normalised fluorescence FNorm [$^{0}/_{00}$] is plotted as a function of [CcdB]. For each capillary (each measuring point), an MST trace is recorded. All traces are then normalised to start at 1000. For each trace, the FNorm value for the dose- response curve is calculated from Fhot (MST laser on)/Fcold (MST laser off). The dissociation constants (K_D) listed in Table S1, were determined employing standard data analysis with MO.Affinity Analysis Software (84). (D) Equilibrium GdnCl denaturation profile of 5 µM of Gyrase A-14 carried out in 1XPBS, pH 7.5 at 25 °C using nanoDSF. The experimental data is shown in black dots, while the fit is shown in a red line. The Cm of Gyrase is 4.48 M thus proving it to be stable and folded in the MST studies carried out in the presence of 1.5 M GdnCl.

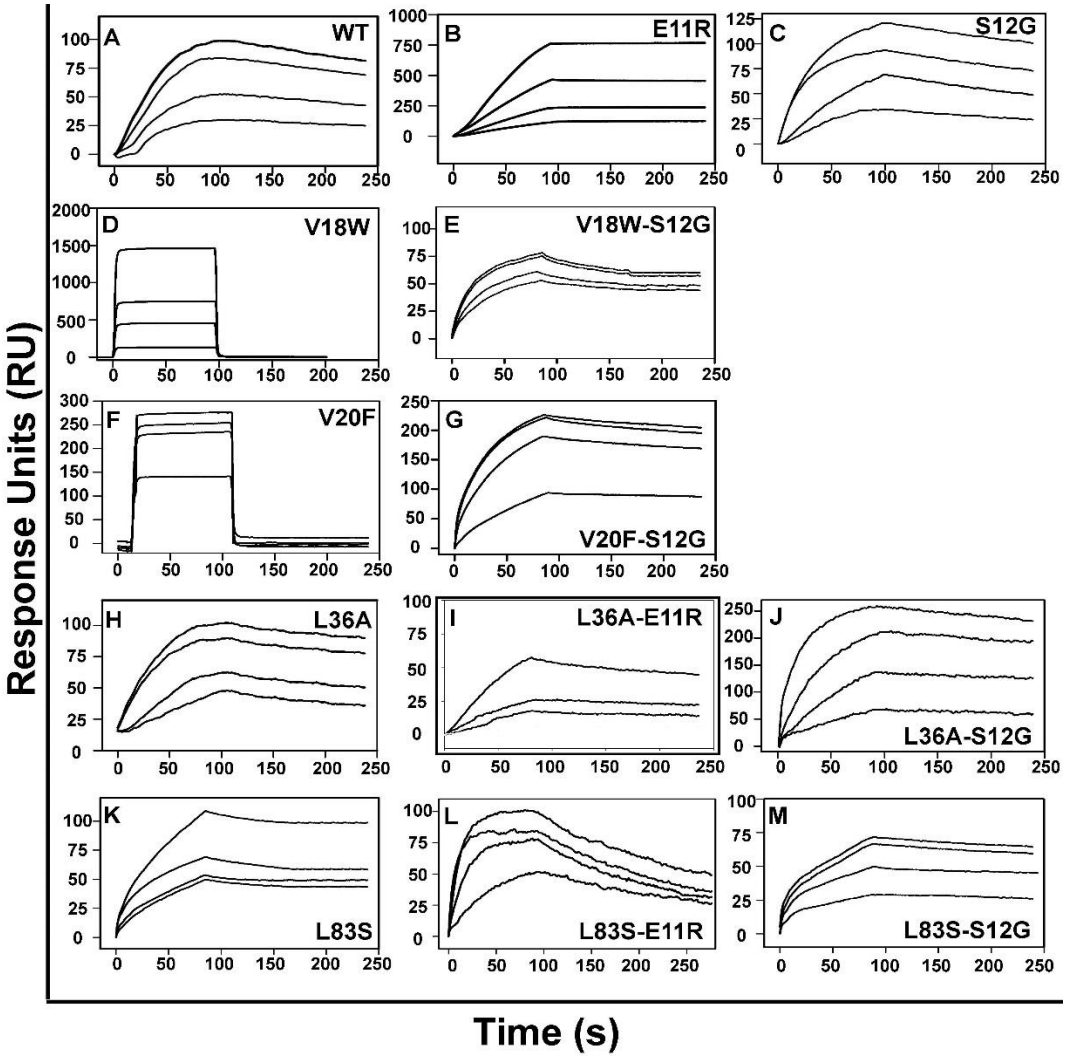

Supplementary Figure S4: Binding of GyraseA-14 to CcdB proteins (related to Figure 2). Overlays show the binding kinetics with analyte concentration increasing from the bottom to the top curve in all cases of (A) WT CcdB (3, 6, 12.5, 25 nM); (B) E11R (50, 100, 200, 500 nM); (C) S12G (3, 6, 25, 50 nM); (D) V18W (200, 500, 1000, 2000 nM); (E) V18W-S12G (200, 500, 1000, 2000 nM); (F) V20F (200, 1000, 2000, 5000 nM); (G) V20F-S12G (100, 200, 500, 1000 nM) ; (H) L36A (12.5, 25, 100, 200 nM); (I) L36A-E11R (10, 21.4, 32, 64.2 nM); (J) L36A-S12G (3, 6, 12.5, 25 nM); (K) L83S (200, 500, 1000, 2000 nM); (L) L83S-E11R (50, 100, 200, 500 nM); (M) L83S-S12G (200, 500, 1000, 2000 nM). The ligand GyraseA-14 was immobilized on the CM5 chip by standard amine coupling. Binding was measured by passing varying concentrations of the analyte (CcdB proteins) over the ligand (GyraseA-14) immobilised chip and the data was fitted to the 1:1 Langmuir Interaction model to obtain the kinetic parameters (Table S1).

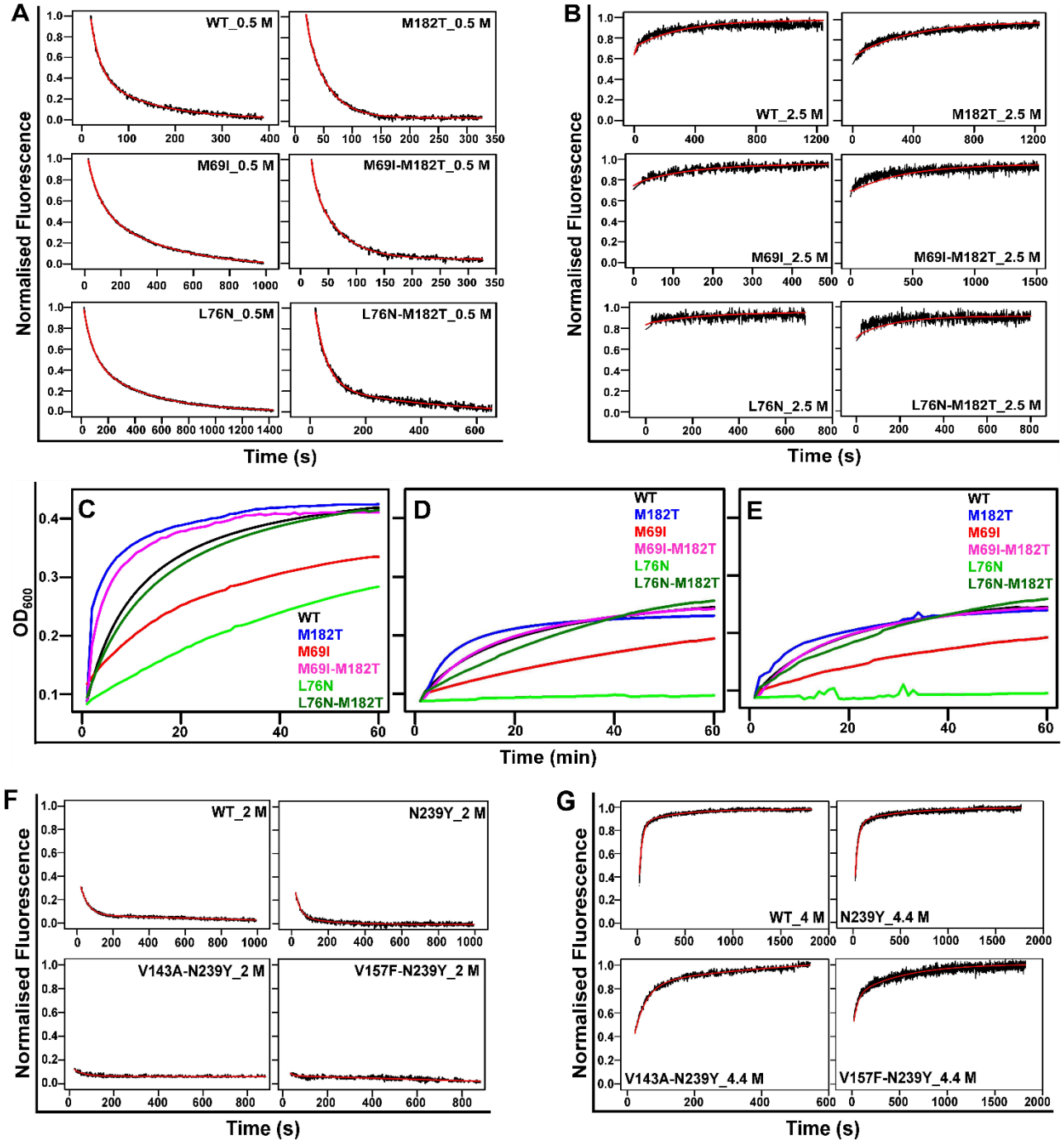

Supplementary Figure S5: Refolding and unfolding kinetics, and hydrolysis activities of TEM-1 β-lactamase mutant proteins (related to Figure 4) as well as refolding and unfolding kinetics of p53-DBD mutant proteins (related to Figure 5). (A) TEM-1 proteins exhibit biphasic refolding kinetics with a fast and slow phase whereas (B) unfolding follows single exponential kinetics. Representative kinetic traces at 5 μM protein concentrations of WT and TEM-1 mutants are shown in presence of 0.5 M GdnCl for refolding and 2.5 M GdnCl for unfolding. The experimental kinetic traces

obtained at the indicated GdnCl concentration are shown in black, while the fits are shown in red**.** The measured kinetic parameters are listed in Table S6. The lactamase activities of the WT and mutants in the following conditions – (C) native, (D) native proteins in 0.5 M GdnCl and (E) refolded proteins in 0.5 M GdnCl, were assayed by observing the rate of nitrocefin hydrolysis (50 μM) at 486 nm at 25 °C at a protein concentration of 10 nM. The M182T suppressor rescues the activity of M69I and L76N mutants. (F) p53-DBD proteins exhibit biphasic refolding kinetics with a significant burst, fast and slow phase whereas (G) unfolding of p53-DBD follows biphasic exponential kinetics with fast and slow phases. Representative kinetic traces at 5 μM protein concentration of WT and p53-DBD mutants are shown in the presence of 2 M Urea for refolding and 4.4 M Urea for unfolding. The experimental kinetic traces obtained are shown in black, while the fits are shown in red**.** The measured kinetic parameters are listed in Table S7.

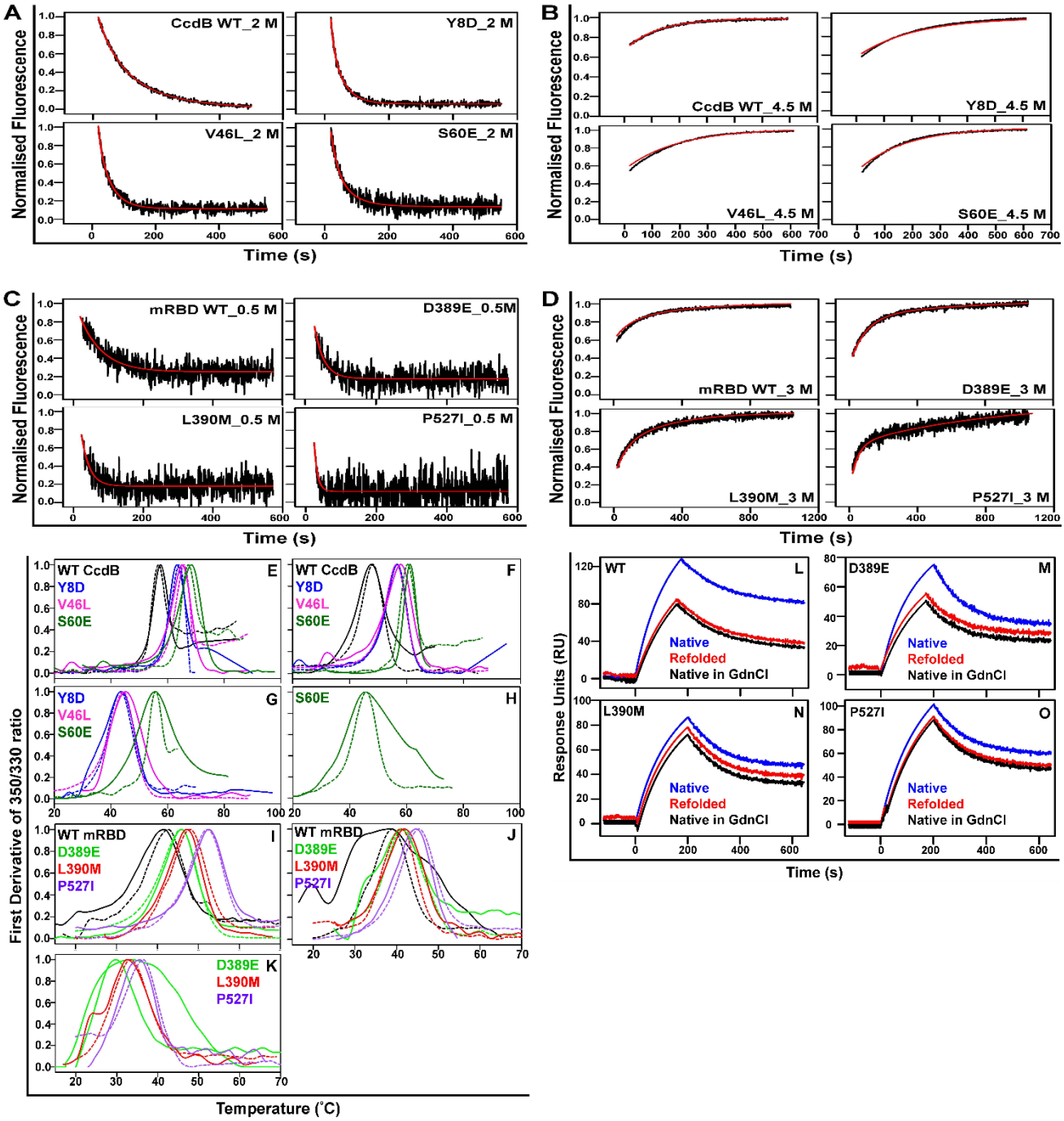

Supplementary Figure S6: Refolding and unfolding kinetics, and thermal denaturation studies of stabilised CcdB and mRBD proteins with suppressor mutations; binding studies of the mRBD proteins to ACE2-hFc neutralizing antibody (related to Figure 6). (A) Biphasic refolding kinetics with a fast and slow phase and (B) single exponential unfolding kinetics of CcdB mutant proteins. Representative kinetic traces at 5 μM protein concentration of WT CcdB; Y8D; V46; S60E are shown. (C) mRBD proteins exhibit single phase refolding kinetics with a significant burst phase whereas (D)

unfolding of mRBD proteins follows biphasic exponential kinetics with burst, fast and slow phases. Representative kinetic traces at 5 µM protein concentration of WT mRBD; D389E; L390M; P527I are shown. The experimental kinetic traces obtained at different GdnCl concentrations are shown in black, while the fits are shown in red**.** The measured kinetic parameters are listed in Tables S9 for CcdB and mRBD mutants.

(E-H) Thermal denaturation traces of 5 µM of native CcdB proteins in (E) 1 M, (F) 2 M, (G) 3 M and (H) 4 M GdnCl (represented by dashed lines) and refolded CcdB proteins in the same concentrations of GdnCl (represented by solid lines). WT CcdB failed to show any transition at 3 M, whereas Y8D and V46L failed to show a thermal unfolding transition at 4 M. S60E showed a thermal transition at 4 M. (I-K) Thermal denaturation traces of 5 µM of native mRBD proteins in (I) 0.5 M, (J) 1 M and (K) 2 M (represented by dashed lines) and refolded mRBD proteins in same concentrations of GdnCl (represented by solid lines). mRBD WT failed to show any transition at 2 M, whereas the stabilised mutants show thermal unfolding upto 2M GdnCl. (L-O) Overlays show the ACE2-hFc binding of the WT and mRBD mutants in the following conditions – native, native in 0.5 M GdnCl and refolded in 0.5 M GdnCl for (L) WT mRBD, (M) D389E, (N) L390M and (O) P27I. The ligand ACE2-hFc was immobilized on Protein-G immobilised GLM sensor chip. Binding was measured by passing 50 nM of the analyte (mRBD proteins) over the ligand (ACE2-hFc) immobilised chip.

Supplementary Table S1 (Related to Figure 1). Fractional solubilities, thermal stabilities (determined by nanoDSF) and GyrA14 binding affinities (determined by SPR and MST) of different CcdB mutants[1]. Binding affinities of refolded proteins and proteins in GdnCl were also measured by MST. SPR experiments were carried out at 25 °C, pH 7.4 and MST experiments were carried out at 25 °C, pH 8.4.

Mutants	Fraction Soluble	T_m (°C)	K_D (nM) SPR	MST Studies		
				K_D (nM) Native	K_D (nM) Native in GdnCl	K_D (nM) Refolded
WT	1.0	66±0.8	1.4±0.6	2.2±0.6	41.8±3.2	32.2±2.7
E11R	0.9	64±1.0	2.5±0.3	1.2±0.3	3.2±0.3	2.4±0.4
S12G	0.9	68±0.8	2.6±1.4	2.3±0.8	74.5±10	99±15
V18W	0.2	54±09	NB	2046.9±132	2241.8[3]±168	2577.4[a]±196
V18W-E11R[2]	0.6	-	-	-	-	-
V18W-S12G	0.6	66±0.9	57±13.2	30.2±4	132.2±12	149.3±16
V20F	0.3	47±0.8	NB	623.5±92	1465.1[4]±117	1078.0[b]±102
V20F-E11R[2]	0.5	-	-	-	-	-
V20F-S12G	0.4	60±0.8	12.7±4	20.9±12	130.9±48	103.6±29
L36A	0.3	58±1.0	9.5±4	17.5±7	125.2±30	162.0±54
L36A-E11R	0.6	63±1.0	3.0±1.3	13±1.3	16.0 ±1.3	1.3±1.0
L36A-S12G	0.7	63±0.2	0.4±0.7	0.3±1.4	1.5±0.6	2.3±2
L83S	0.4	59±0.8	75.0±15.3	88.7±19	175.3±63	199.4±45
L83S-E11R	0.5	67±0.5	6.8±2.9	0.30±0.1	16±2.9	0.4±0.1
L83S-S12G	0.5	66±0.7	7.2±11.3	4.12±2.3	11.9±9.4	13±7.2

[1]Reported standard errors are derived from two independent experiments, each performed in duplicates.

[2]Mutants could not be purified.

[3,4] Refolded in 0.1 M GdnCl. All the other proteins were refolded in 1.5 M GdnCl.

NB: No Binding.

Supplementary Table S2 (Related to Figure 2). Kinetic Parameters for refolding and unfolding of CcdB mutants measured under different buffer conditions at 25 °C, pH 8.4[1].

Mutant	[GdnCl] (Refold/ Unfold) (M)	Refolding					Unfolding		
		Fast Phase			Slow Phase		A0	A1	ku_1 (s^{-1})
		a0	a1	kf_1 (s^{-1})	a2	kf_2 (s^{-1})			
WT	**(1.5/3.5)**	0.02± 0.02	0.55± 0.03	0.027 ±0.02	0.43± 0.03	0.002± 0.001	0.60± 0.03	0.40± 0.01	0.05± 0.05
E11R	**(1.5/3.5)**	0.14± 0.03	0.44± 0.08	0.080 ±0.01	0.42± 0.04	0.02± 0.0066	0.51± 0.04	0.49± 0.04	0.04± 0.08
S12G	**(1.5/3.5)**	0.03± 0.03	0.79± 0.02	0.041 ±0.05	0.18± 0.02	0.001± 0.003	0.44± 0.02	0.56± 0.03	0.03± 0.03
V18W	**(0.5/2.0)**	0.03± 0.06	0.52± 0.03	0.030 ±0.03	0.45± 0.06	0.003± 0.01	0.63± 0.09	0.37± 0.09	0.29± 0.03
V18W-S12G	**(0.5/2.0)**	0.20± 0.01	0.40± 0.08	0.095 ±0.13	0.40± 0.06	0.015± 0.044	0.46± 0.03	0.54± 0.03	0.10± 0.05
V20F	**(0.5/2.0)**	0.02± 0.05	0.71± 0.06	0.024 ±0.01	0.27± 0.06	0.002± 0.07	0.76± 0.01	0.24± 0.01	0.44± 0.08
V20F-S12G	**(0.5/2.0)**	0.02± 0.07	0.67± 0.15	0.104 ±0.09	0.31± 0.08	0.02± 0.002	0.66± 0.04	0.34± 0.03	0.16± 0.04
L36A	**(1.0/3.5)**	0.05± 0.09	0.55± 0.04	0.016 ±0.08	0.40± 0.08	0.001± 0.001	0.77± 0.08	0.27± 0.09	0.24± 0.02
L36A-E11R	**(1.0/3.5)**	0.10± 0.02	0.53± 0.03	0.046 ±0.02	0.36± 0.03	0.001± 0.001	0.61± 0.01	0.39± 0.01	0.17± 0.08
L36A-S12G	**(1.0/3.5)**	0.10± 0.01	0.54± 0.07	0.064 ±0.01	0.34± 0.05	0.007± 0.0066	0.64± 0.02	0.36± 0.02	0.07± 0.03
L83S	**(1.0/3.5)**	0.03± 0.01	0.62± 0.01	0.032 ±0.05	0.35± 0.02	0.004± 0.006	0.77± 0.03	0.23± 0.03	0.28± 0.09
L83S-E11R	**(1.0/3.5)**	0.62±0. 04	-	-	0.38± 0.04	0.035± 0.001	0.72± 0.01	0.28± 0.02	0.10± 0.03
L83S-S12G	**(1.0/3.5)**	0.02± 0.07	0.62± 0.02	0.096 ±0.08	0.36± 0.01	0.012± 0.01	0.71± 0.06	0.29± 0.06	0.15± 0.08

[1]Reported standard errors are derived from two independent experiments, each performed in duplicates.

Supplementary Table S3 (Related to Figure 2). Relative Kinetic Parameters for *in vitro* Refolding and Unfolding of CcdB mutants extrapolated to zero denaturant[1].

Mutants	Refolding				Unfolding	
	Fast Phase		Slow Phase		m value ($M^{-1}s^{-1}$)	rate constant[2] (s^{-1})
	m value (M^{-1})	rate constant[2] (s^{-1})	m value (M^{-1})	rate constant[2] (s^{-1})		
WT	0.29±0.004	0.44±0.04	0.03±0.002	0.05±0.01	0.02±0.002	0.005±0.01
E11R	0.58±0.005	0.94±0.009	0.09±0.003	0.15±0.02	0.02±0.003	0.002±0.02
S12G	0.52±0.010	0.81±0.12	0.08±0.001	0.13±0.008	0.02±0.001	0.002±0.008
V18W	0.06±0.005	0.06±0.001	9e-3±0.003	7e-3±0.001	0.35±0.08	0.032±0.08
V18W-S12G	0.20±0.009	0.19±0.01	0.03±0.004	0.06±0.004	0.14±0.004	0.019±0.004
V20F	0.03±0.006	0.04±0.004	4e-3±0.002	4e-3±0.001	0.45±0.08	0.045±0.01
V20F-S12G	0.26±0.09	0.23±0.12	0.04±0.03	0.04±0.01	0.16±0.004	0.015±0.01
L36A	0.10±0.02	0.11±0.05	0.01±0.01	0.01±0.02	0.12±0.03	0.019±0.04
L36A-E11R	0.21±0.02	0.26±0.03	0.03±0.01	0.03±0.01	0.06±0.0001	0.011±0.003
L36A-S12G	0.39±0.007	0.44±0.01	0.06±0.002	0.06±0.04	0.05±0.001	0.010±0.001
L83S	0.13±0.02	0.17±0.03	0.02±0.002	0.02±0.003	0.11±0.003	0.012±0.02
L83S-E11R	-[3]	-[3]	0.10±0.003	0.16±0.01	0.04±0.0008	0.004±2e-3
L83S-S12G	0.50±0.005	0.60±0.057	0.09±0.003	0.10±0.004	0.06±0.02	0.006±0.001

[1]Reported standard errors are derived from two independent experiments, each performed in duplicates.

[2]Reported rate constants are extrapolated to 0 M GdnCl for relative comparison among different mutants.

[3] Fast phase of refolding couldn't be captured.

Supplementary Table S4 (Related to Figure 2, S1). Top: Thermodynamic parameters (C_m, ΔG^0, m), apparent thermal stability (T_m), thermal stabilities of refolded and native proteins in presence of 1.5 M GdnCl ($T_{mRefold}$, T_{mGdnCl}). **Bottom:** Kinetic parameters for refolding and unfolding of CcdB WT and E11R in 1.5 M and 4 M GdnCl respectively of CcdB WT and E11R carried out in 1X PBS at 25 °C[1].

Mutants	**C_m (M)**	**ΔG^0 (kcal.mol^{-1})**	**m (kcal.mol^{-1}M^{-1})**	**T_m (°C)**	**$T_{mRefold}$ (°C)**	**T_{mGdnCl} (°C)**
WT	2.9±0.2	19.4±0.7	4.2±0.3	65±0.6	56±0.5	57±0.5
E11R	2.8±0.1	18.7±1.0	4.1±0.5	64±0.8	55±0.6	56±0.6

Mutants	**Refolding**					**Unfolding**		
	Fast Phase			**Slow Phase**		**A0**	**A1**	**ku_1 (s^{-1})**
	a0	**a1**	**kf_1 (s^{-1})**	**a2**	**kf_2 (s^{-1})**			
WT	0.03± 0.001	0.56± 0.03	0.044 ±0.004	0.41± 0.04	0.015± 0.0003	0.58± 0.02	0.42± 0.01	0.017± 0.001
E11R	0.08± 0.001	0.53± 0.02	0.09 ±0.01	0.39± 0.04	0.024± 0.001	0.57± 0.009	0.43± 0.04	0.016± 0.002

[1]Reported standard errors are derived from two independent experiments, each performed in duplicates.

Supplementary Table S5 (Related to Figure 2). Thermodynamic stability parameters, following chemical denaturation and melting temperatures of refolded and native proteins in presence of 1.5 M GdnCl ($T_{mRefold}$, T_{mGdnCl}) determined by nanoDSF, of different CcdB mutants[1]. Residual activity after high temperature incubation of CcdB mutants was determined by SPR at room temperature.

Mutants	**C_m (M)**	**ΔG^0 (kcal.mol^{-1})**	**m (kcal.mol^{-1}M^{-1})**	**$T_{mRefold}$ (°C)**	**T_{mGdnCl} (°C)**	**Residual activity (%)**	
						40 °C	**80 °C**
WT	2.8±0.1	21.1±0.7	4.97±0.5	53±0.5	52±0.8	24	0.8
E11R	2.3±0.2	18.0±1.8	4.55±0.5	55±0.4	55±0.5	1.2	0.6
S12G	3.0±0.3	21.9±1.4	4.90±0.2	55±0.9	55±1.4	61	3.7
V18W	0.8±0.7	11.0±1.8	4.00±1.2	[2]	[2]	-	-
V18W-S12G	1.3±0.09	13.5±0.8	4.87±0.2	45±0.4	43±0.9	-	-
V20F	0.3±0.02	8.6±1.8	4.06±0.2	[3]	[3]	-	-
V20F-S12G	1.0±0.4	12.1±1.4	4.88±0.2	43±1.2	43±0.6	-	-
L36A	1.5±0.4	13.9±0.3	4.45±1.4	45±1.4	46±0.9	11.7	0.4
L36A-E11R	2.4±0.4	18.9±1.2	4.50±0.5	51±0.8	51±0.4	34	2.4
L36A-S12G	2.4±0.3	18.8±0.9	4.82±0.7	52±1.2	51±0.6	47.6	9.1
L83S	1.6±0.1	14.4±1.7	4.43±0.8	43±0.2	41±1.8	-	-
L83S-E11R	2.1±0.2	18.3±3.2	4.73±0.5	54±0.1	53±0.6	-	-
L83S-S12G	2.3±0.9	18.6±1.3	4.70±0.9	55±0.9	55±0.6	-	-

[1]Reported standard errors are derived from two independent experiments, each performed in duplicates.

[2,3] Could not be refolded in 1.5 M GdnCl. All the other proteins were refolded in 1.5 M GdnCl.

-Not determined.

Supplementary Table S6 (Related to Figure 4). Top: MIC and IC_{90} for ampicillin and cefotaxime from OD_{600} and plate data measurements, thermodynamic stability parameters (C_m, ΔG^0, m), apparent thermal stability (T_m), thermal stabilities of refolded proteins and native proteins in presence of 0.5 M GdnCl ($T_{mRefold,}$, T_{mGdnCl}), of different TEM-1 β-lactamase mutants[1]. **Bottom:** Kinetic Parameters for refolding and unfolding of TEM-1 β-lactamase mutants measured in 0.5 M and 2.5 M GdnCl respectively carried out in 10 mM HEPES, 300 mM NaCl, 10% glycerol, pH 7.0, at 25 °C[1].

Mutants	**Ampicillin (µg/mL)**		**Cefotaxime (µg/mL)**		**C_m (M)**	**ΔG^0 (kcal.mol^{-1})**	**m (kcal.mol^{-1}M^{-1})**	**T_m (°C)**	**$T_{mRefold}$ (°C)**	**$T_{mGdnCl,}$ (°C)**
	MIC	**IC_{90}**	**MIC**	**IC_{90}**						
WT	≈3000	4000	16	10	1.2±0.1	2.9±0.5	2.4±0.1	51±0.2	41±0.4	41±0.2
M182T	≈3000	4000	16	15	1.9±0.3	4.7±0.6	3.1±0.3	57±0.1	47±0.3	48±0.5
M69I	≈800	1000	8	6	0.6±0.1	2.0±0.2	2.1±0.2	47±0.3	31±0.1	32±0.4
M69I-M182T	≈800	1000	8	6	1.4±0.2	4.0±0.3	2.8±0.1	54±0.2	44±0.2	44±0.3
L76N	≈50	20	2	<1	0.5±0.1	1.1±0.1	1.8±0.2	40±0.5	NT	NT
L76N-M182T	≈1500	1500	4	4	1.1±0.2	2.8±0.3	2.3±0.4	48±0.3	39±0.1	39±0.5

Mutants	**Refolding**					**Unfolding**		
	Fast Phase			**Slow Phase**		**A0**	**A1**	**ku_1 (s^{-1})**
	a0	**a1**	**kf_1 (s^{-1})**	**a2**	**kf_2 (s^{-1})**			
WT	0.01±0.02	0.51±0.03	0.049±0.01	0.48±0.03	0.004±0.001	0.65±0.03	0.35±0.01	0.03±0.003
M182T	0.03±0.03	0.53±0.08	0.19±0.01	0.44±0.04	0.008±0.001	0.56±0.04	0.44±0.04	0.02±0.002
M69I	0.03±0.03	0.55±0.02	0.016±0.01	0.42±0.02	0.003±0.004	0.71±0.02	0.29±0.03	0.07±0.003
M69I-M182T	0.03±0.06	0.52±0.03	0.11±0.02	0.45±0.06	0.006±0.001	0.65±0.09	0.35±0.09	0.03±0.001
L76N	0.02±0.01	0.60±0.08	0.014±0.01	0.38±0.06	0.002±0.002	0.79±0.03	0.21±0.03	0.10±0.004
L76N-M182T	0.03±0.05	0.68±0.06	0.023±0.02	0.29±0.06	0.003±0.001	0.68±0.01	0.32±0.01	0.06±0.003

[1]Reported standard errors are derived from two independent experiments, each performed in duplicates.

NT- No Transition: Not refolded in 0.5 M GdnCl. All the other proteins were refolded in 0.5 M GdnCl.

Supplementary Table 7 (Related to Figure 5). Top: Fractional solubilities, thermodynamic stability parameters (C_m, ΔG^0, m), apparent thermal stabilities (T_m), thermal stabilities of refolded and native proteins in the presence of 0.5 M Urea ($T_{mRefold}$,$T_{m,urea}$) determined by nanoDSF, of different p53 mutants[1]. **Bottom:** Kinetic Parameters for refolding and unfolding of p53 mutants measured in 2 M and 4.4 M Urea respectively carried out in 50 mM NaH_2PO_4, 500 mM NaCl, 500 mM imidazole, 10 mM DTT, pH 7.2 at 15 °C[1].

Mutants	**Fraction soluble**	**C_m (M)**	**ΔG^0 (kcal.mol^{-1})**	**m (kcal.mol^{-1}M^{-1})**	**T_m (°C)**	**$T_{m,refold}$ (°C)**	**$T_{m,urea}$ (°C)**
WT	0.4±0.05	2.8±0.02	2.5±0.1	0.9±0.01	30±0.1	29±0.1	29±0.1
N239Y	0.5±0.05	3.0±0.05	2.6±0.2	0.9±0.02	32±0.1	29±0.4	30±0.1
V143A	0.1±0.04	ND	ND	ND	ND	ND	ND
V143A-N239Y	0.3±0.02	3.1±0.1	2.7±0.1	0.9±0.002	31±0.1	29±0.1	27±0.1
V157F	0.1±0.05	ND	ND	ND	ND	ND	ND
V157F - N239Y	0.4±0.04	3.3±0.05	2.9±0.1	0.9±0.005	33±0.1	32±0.1	32±0.1

Mutants	**Refolding**					**Unfolding**				
	Fast Phase			**Slow Phase**		**A0**	**A1**	**ku_1 (s^{-1})**	**A2**	**ku_2 (s^{-1})**
	a0	**a1**	**kf_1 (s^{-1})**	**a2**	**kf_2 (s^{-1})**					
WT	0.68± 0.01	0.14± 0.0004	0.024 ±0.0003	0.18± 0.005	0.0003± 0.00001	0.35± 0.01	0.53± 0.01	0.046± 0.0005	0.12± 0.002	0.003± 0.00005
N239Y	0.73± 0.002	0.14± 0.0004	0.037 ±0.0003	0.13± 0.007	0.006± 0.005	0.32± 0.009	0.56± 0.009	0.037± 0.0006	0.12± 0.002	0.0025± 0.00007
V143A N239Y	0.86± 0.003	0.05± 0.0003	0.023 ±0.003	0.09± 0.005	0.003± 0.006	0.40± 0.01	0.37± 0.01	0.028± 0.001	0.23± 0.007	0.0017± 0.0005
V157F N239Y	0.87± 0.002	0.02± 0.001	0.083 ±0.04	0.11± 0.002	0.0004± 0.00001	0.49± 0.003	0.23± 0.003	0.023± 0.0015	0.28± 0.003	0.0019± 0.00006

[1]Reported standard errors are derived from two independent experiments, each performed in duplicates.
ND – Not determined as the corresponding proteins could not be purified.

Supplementary Table 8 (Related to Figure 6). Thermodynamic parameters (C_m, ΔG^0, m), determined by nanoDSF, of CcdB and mRBD mutants[1].

Mutants	**C_m (M)**		**ΔG^0 (kcal.mol^{-1})**		**m (kcal.mol^{-1}M^{-1})**	
CcdB WT	2.8±0.1		21.1±0.7		4.97±0.5	
CcdB Y8D	3.1±0.3		22.7±1.2		5.00±0.1	
CcdB V46L	3.2±0.3		23.2±1.4		5.01±0.3	
CcdB S60E	3.5±0.5		24.8±1.1		5.03±0.2	
Mutants	**C_{mN-I} (M)**	**C_{mI-U} (M)**	**ΔG_{N-I}^0 (kcal.mol^{-1})**	**ΔG_{I-U}^0 (kcal.mol^{-1})**	**m_{N-I} (kcal.mol^{-1}M^{-1})**	**m_{I-U} (kcal.mol^{-1}M^{-1})**
mRBD WT	1.2±0.2	2.4±0.1	2.3±0.5	2.4±0.6	1.3±0.1	1.2±0.2
mRBD D389E	1.5±0.3	2.6±0.3	2.7±0.6	2.6±0.8	1.3±0.1	1.2±0.2
mRBD L390M	1.6±0.2	2.7±0.1	2.8±0.4	2.6±0.4	1.4±0.2	1.3±0.2
mRBD P527I	1.8±0.4	2.8±0.4	3.0±0.3	2.8±0.7	1.4±0.3	1.3±0.2

[1]Reported standard errors are derived from two independent experiments, each performed in duplicates.

Supplementary Table S9 (Related to Figure 6). Top: Kinetic Parameters for refolding and unfolding of stabilised CcdB mutants measured in 2 M and 4.5 M GdnCl respectively, carried out in 200 mM HEPES, pH 8.4 at 25 °C[1]. **Bottom:** Kinetic Parameters for refolding and unfolding of stabilised mRBD mutants in 0.5 M and 3 M GdnCl respectively, carried out in 1XPBS, pH 7.0 at 25 °C[1].

Mutants	**Refolding (2 M)**					**Unfolding (4.5 M)**		
	Fast Phase			**Slow Phase**				
	a0	**a1**	**kf_1 (s^{-1})**	**a2**	**kf_2 (s^{-1})**	**A0**	**A1**	**ku_1 (s^{-1})**
CcdB WT	0.02± 0.02	0.55± 0.03	0.027 ±0.02	0.43± 0.03	0.002± 0.001	0.73± 0.03	0.27± 0.01	0.060± 0.05
CcdB Y8D	0.01± 0.02	0.51± 0.03	0.06 ±0.01	0.48± 0.03	0.018± 0.001	0.58± 0.03	0.42± 0.01	0.027± 0.003
CcdB V46L	0.03± 0.03	0.53± 0.08	0.10 ±0.01	0.44± 0.04	0.026± 0.001	0.55± 0.04	0.45± 0.04	0.025± 0.002
CcdB S60E	0.03± 0.03	0.55± 0.02	0.13 ±0.01	0.42± 0.02	0.028± 0.004	0.52± 0.02	0.48± 0.03	0.020± 0.003

Mutants	**Refolding (0.5 M)**			**Unfolding (3 M)**				
				Fast Phase			**Slow Phase**	
	a0	**a1**	**kf_1 (s^{-1})**	**A0**	**A1**	**ku_1 (s^{-1})**	**A2**	**ku_2 (s^{-1})**
mRBD WT	0.20± 0.01	0.80± 0.02	0.015 ±0.003	0.58± 0.02	0.28± 0.03	0.051 ±0.002	0.14± 0.03	0.002± 0.0005
mRBD D389E	0.26± 0.03	0.74± 0.01	0.038 ±0.004	0.42± 0.03	0.48± 0.08	0.016 ±0.003	0.10± 0.04	0.001± 0.0006
mRBD L390M	0.25± 0.02	0.75± 0.03	0.044 ±0.002	0.43± 0.03	0.47± 0.08	0.014 ±0.001	0.12± 0.04	0.001± 0.001
mRBD P527I	0.35± 0.02	0.65± 0.01	0.103 ±0.01	0.33± 0.03	0.52± 0.02	0.013 ±0.002	0.15± 0.02	0.001± 0.0007

[1]Reported standard errors are derived from two independent experiments, each performed in duplicates.

Supplementary Table S10 (Related to Figure 7). Data collection and refinement statistics for CcdB mutants.

Data collection	**S12G**	**V46L**	**S60E**
Space group	I2	C2	C2
a, b, c (Å)	35.57, 36.53, 67.53	75.10, 36.76, 35.91	74.81, 36.64, 35.67
α, β, γ (°)	90, 93.69, 90	90, 115.19, 90	90, 114.97, 90
Wavelength (Å)	1.5418	1.0358	1.5418
Resolution range (Å)	33.69 – 1.63 (1.72 – 1.63)	33.98-1.35 (1.43-1.35)	10.00-1.93 (2.03-1.93)
Total No. of reflections	48336 (6679)	114256 (14182)	22462 (2937)
No. of unique reflections	9822 (1360)	19433 (2799)	6557 (890)
Multiplicity	4.9 (4.9)	5.9 (5.1)	3.4 (3.3)
Completeness (%)	90.6 (86.9)	100 (100)	97.5 (91.6)
⟨I/σ(I)⟩	9.8 (4.8)	11.6 (3.7)	9.6 (3.8)
Wilson B factor (Å^2)	11.66	5.78	8.6
$R_{p.i.m.}$	0.041 (0.097)	0.043 (0.141)	0.081 (0.268)
R_{merge}	0.083 (0.195)	0.098 (0.288)	0.130 (0.424)
R_{meas}	0.093 (0.218)	0.108 (0.322)	0.154 (0.504)
CC1/2	0.995 (0.967)	0.994 (0.928)	0.99 (0.801)
Refinement			
R_{work} (%)	22.8	16.2	17.0
R_{free} (%)	26.9	18.4	21.4
RMSD			
Bond (Å)	0.0072	0.0138	0.0051
Angle (°)	1.4844	1.9222	1.3247
Ramachandran plot			
Ramachandran favoured (%)	98	100.0	99
Ramachandran allowed (%)	2	0	1
Ramachandran outliers (%)	0	0	0
Average B factor (Å^2)			
Overall	18.85	11.19	11.37
Protein	18.05	9.13	10.57
Solvent	25.77	21.25	18.08
Other	17.70	8.71	11.53
Total no of atoms			
Protein atoms	816	814	820
Solvent	95	167	98
Other	2 Cl^-	2 Cl^-	2 Cl^-
Z	1	1	1

* : values within brackets are for highest resolution shell.